Dynamics of the middle atmosphere as simulated by the Whole Atmosphere Community Climate Model, version 3 (WACCM3)

Jadwiga H. Richter,[1] Fabrizio Sassi,[1] Rolando R. Garcia,[2] Katja Matthes,[2] and Chris A. Fischer[1]

Received 10 August 2007; revised 14 November 2007; accepted 7 January 2008; published 16 April 2008.

[1] The Whole Atmosphere Community Climate Model, version 3 (WACCM3) is a state-of-the-art climate model extending from the Earth's surface to the lower thermosphere. In this paper we present a detailed climatology of the dynamics of the middle atmosphere as represented by WACCM3 at various horizontal resolutions and compare them to observations. In addition to the mean climatological fields, we examine in detail the middle atmospheric momentum budget as well as several lower and upper atmosphere coupling phenomena including stratospheric sudden warmings, the 2-day wave, and the migrating diurnal tide. We find that in large part, differences between WACCM3 and observations and the mean state of the model at various horizontal resolutions are related to gravity wave drag, which is parameterized in WACCM3 (and similar models). All three lower and upper atmosphere coupling processes examined show high sensitivity to the model's resolution.

Citation: Richter, J. H., F. Sassi, R. R. Garcia, K. Matthes, and C. A. Fischer (2008), Dynamics of the middle atmosphere as simulated by the Whole Atmosphere Community Climate Model, version 3 (WACCM3), *J. Geophys. Res.*, *113*, D08101, doi:10.1029/2007JD009269.

1. Introduction

[2] The Whole Atmosphere Community Climate Model, version 3 (WACCM3) is a state-of-the-art climate model extending from the Earth's surface to the lower thermosphere. This model is one of a few high-top general circulations models (GCMs), including the Hamburg Model of the Neutral and Ionized Atmosphere (HAMMONIA) [*Schmidt et al.*, 2006] and the extended Canadian Middle Atmosphere Model (CMAM) [*Fomichev et al.*, 2002], which allow for studies of chemical, dynamical, and radiative coupling processes between the lower and upper atmosphere. These "high-top" GCMs can be used to study problems such as the solar influence on Earth's climate [e.g., *Schmidt et al.*, 2006; *Marsh et al.*, 2007], constituent transport and trends in the middle atmosphere [*Garcia et al.*, 2007], the influence of the stratosphere on the tropospheric climate [*Baldwin and Dunkerton*, 1999], and the connection between climate change and polar mesospheric clouds [*Thomas*, 2003; *Shettle et al.*, 2002].

[3] Many of the coupling phenomena between the lower and upper atmosphere are dependent on the mean climate and the dynamics of the middle atmosphere, and hence understanding the drivers of middle atmospheric dynamics in high-top GCMs is crucial to the understanding of the coupling between the various atmospheric layers and influences on climate. In the middle atmosphere, one of the most important dynamical drivers are gravity waves, which are parameterized in GCMs. It is important to understand their contribution to the momentum budget relative to the driving from resolved waves. Global dynamical driving by gravity waves can not be determined directly from observations, but efforts can be made to verify with observations the general features of the resolved wave field, such as planetary waves and tides. Once resolved scales have been accounted for, the driving due to gravity waves can be inferred from the unbalanced residual of the momentum budget.

[4] In addition to ambiguities related to gravity wave drag in GCMs, the influence of horizontal model resolution on the resolved wave dynamics of the middle atmosphere is also incompletely understood. *Jablonowski and Williamson* [2006] have shown that proper representation of tropospheric baroclinic waves in GCMs requires horizontal resolution of about 1 to 2°. High-top GCMs, especially those with interactive chemistry such as WACCM3, are extremely computationally expensive, and hence experiments requiring long simulations may need to be run at coarser than desirable resolution. Typically high-top GCMs are run at the equivalent of 2 to 4° horizontal resolution. Impacts of horizontal resolution in these models, as well as consequences of the findings of *Jablonowski and Williamson* [2006] with regards to the middle atmosphere, have not been investigated so far.

[5] In this paper, we present the mean climatology of zonal winds and temperature and we examine in detail the dynamics of the middle atmosphere in WACCM3 at three different resolutions: 1° × 1.25°, 1.9° × 2.5°, and 4° × 5°. Where possible, we evaluate the model against observations

[1] Climate and Global Dynamics Division, National Center for Atmospheric Research, Boulder, Colorado, USA.
[2] Atmospheric Chemistry Division, National Center for Atmospheric Research, Boulder, Colorado, USA.

Copyright 2008 by the American Geophysical Union.
0148-0227/08/2007JD009269

in order to understand the middle atmospheric dynamics in WACCM3. Better understanding of dynamical drivers in WACCM3 should lead to a more complete understanding of the coupling processes between atmospheric layers, and looking at the dynamical processes driving the middle atmosphere at various resolutions should elucidate the possible influence of horizontal resolution on scientific findings with WACCM3.

[6] In this paper we look at selected features of both the stratospheric and mesospheric/lower thermospheric (MLT) dynamics, including the detailed momentum budget. Stratospheric dynamics are typically not given a lot of attention in GCM studies of the MLT region; however, stratospheric dynamics are of great importance to the coupling between the troposphere and the MLT. In particular, gravity wave and resolved wave spectra in the MLT are influenced greatly by stratospheric winds. There is also evidence pointing to the downward coupling between the upper atmosphere and troposphere. *Boville* [1984] showed in a modeling study that changes in the polar night jet lead to significant changes in tropospheric planetary wave structure. *Dunkerton* [2001] showed observational evidence that strong variations in stratospheric circulation can descend into the troposphere and affect weather there. A good diagnostic of the mean state and variability of the stratosphere are stratospheric sudden warmings (SSWs). They are initiated by upward propagating planetary waves that interact with the polar vortex and can influence surface weather patterns [*Polvani and Waugh*, 2004]. Hence, we examine the frequency of stratospheric sudden warmings in WACCM3 and compare it to observations.

[7] In the MLT, we examine which wave modes are the primary contributors to the momentum budget. In addition, we look in detail at the climatology of the migrating diurnal tide and of the quasi-2-day (d) wave. The migrating diurnal tide is the most prominent feature in the MLT during all seasons and it can deposit significant momentum in this region [*Lieberman and Hays*, 1994]. The quasi-2-d wave is believed to be a normal mode of the atmosphere which is typically present only near the solstice [*Salby*, 1981; *Salby and Callaghan*, 2001, 2003]. The 2-d wave can also be a substantial momentum contributor in the MLT [*Norton and Thuburn*, 1996; *Lieberman*, 2002]. The modeling of the quasi-2-d wave poses a greater challenge to GCMs as this wave amplifies in regions of instability and hence its climatology is strongly dependent on the zonal winds in the model.

[8] This paper is organized as follows. Section 2 is a description of WACCM3; section 3 describes the model's climatology; section 4 presents WACCM3's momentum budget; section 5 examines in more detail lower and upper atmospheric coupling phenomena, including SSWs, the quasi-2-d wave, and the migrating diurnal tide, and section 6 includes a discussion and conclusions.

2. Model

[9] WACCM 3 is a vertically extended version of the Community Atmosphere Model, version 3 (CAM3). Previous versions of WACCM include WACCM1, version b (WACCM1b) described by *Sassi et al.* [2002], and WACCM2 described by *Sassi et al.* [2005]. WACCM1b is based on Community Climate System Model, version 3 (CCM3) physics and using the software framework of CAM2. This version of WACCM did not include interactive chemistry. Interactive chemistry was added to WACCM2 which was based on a preliminary version of CAM3. Ion chemistry and other mesospheric/lower thermospheric physics described below were introduced to WACCM3.

[10] WACCM3 uses the finite volume dynamical core of *Lin* [2004] with 66 vertical levels from the ground to 4.5×10^{-6} hPa ($\sim$145 km). The vertical resolution in WACCM3 is variable: 1.1 km in the troposphere above the boundary layer, 1.1–1.4 km in the lower stratosphere, 1.75 km around the stratopause ($\sim$50 km) and 3.5 km above about 65 km. The bottommost 18 vertical levels, up to 100 hPa, are the same as in CAM3; In CAM3 the vertical resolution above 100 hPa up to the model top at 3.5 hPa is very coarse. The horizontal resolution in WACCM3 can be varied. Two standard resolutions are: $1.9^\circ \times 2.5^\circ$ and $4^\circ \times 5^\circ$ (latitude x longitude). Here we also present limited results from a higher-resolution run ($1^\circ \times 1.25^\circ$).

[11] WACCM3 uses all of CAM3's physical parameterizations, which are discussed in detail by *Collins et al.* [2006]. The parameterizations in CAM3 modified for WACCM include the gravity wave drag parameterization and vertical diffusion. In addition, WACCM3 includes a detailed interactive chemistry model for the middle atmosphere, and hence ozone and other species used in radiative calculations are calculated interactively in WACCM, whereas CAM3 uses fixed climatological values. WACCM3 also includes a model of ion chemistry in the mesosphere/lower thermosphere, parameterizations of ion drag and auroral processes, parameterizations of shortwave heating at extreme ultraviolet (EUV) wavelengths, and infrared transfer under nonlocal thermodynamic equilibrium (NLTE) conditions. Below we describe the details of the gravity wave parameterization as they are relevant to the presented results. For a description of other parameterizations unique to WACCM3, the reader is referred to *Garcia et al.* [2007].

[12] WACCM3 includes an orographic gravity wave parameterization based on *McFarlane* [1987] and a nonorographic parameterization based on the formulation of *Lindzen* [1981]. The nonorographic parameterization includes 64 discrete waves with phase speeds between -80 and 80 m s^{-1} with uniform spacing of 2.5 m s^{-1}. The wave source is assumed to be located at the first interface above 500 hPa and to be oriented in the direction of the wind on that interface. The gravity wave source spectrum is specified as a Gaussian in phase speed c, centered on the source wind, U_s:

$$\tau_s(c) = \tau_b \exp\left[-\left(\frac{c - U_s}{c_w}\right)^2\right] \tag{1}$$

where $c_w = 30$ m s^{-1}.

[13] The gravity wave source spectrum is a function of latitude and time of year, specified as:

$$\tau_b = \tau_b^* F(\phi, t) \tag{2}$$

where τ_b* is a constant and $F(\phi,t)$ is a function designed to reproduce the latitude and seasonal behavior of the source

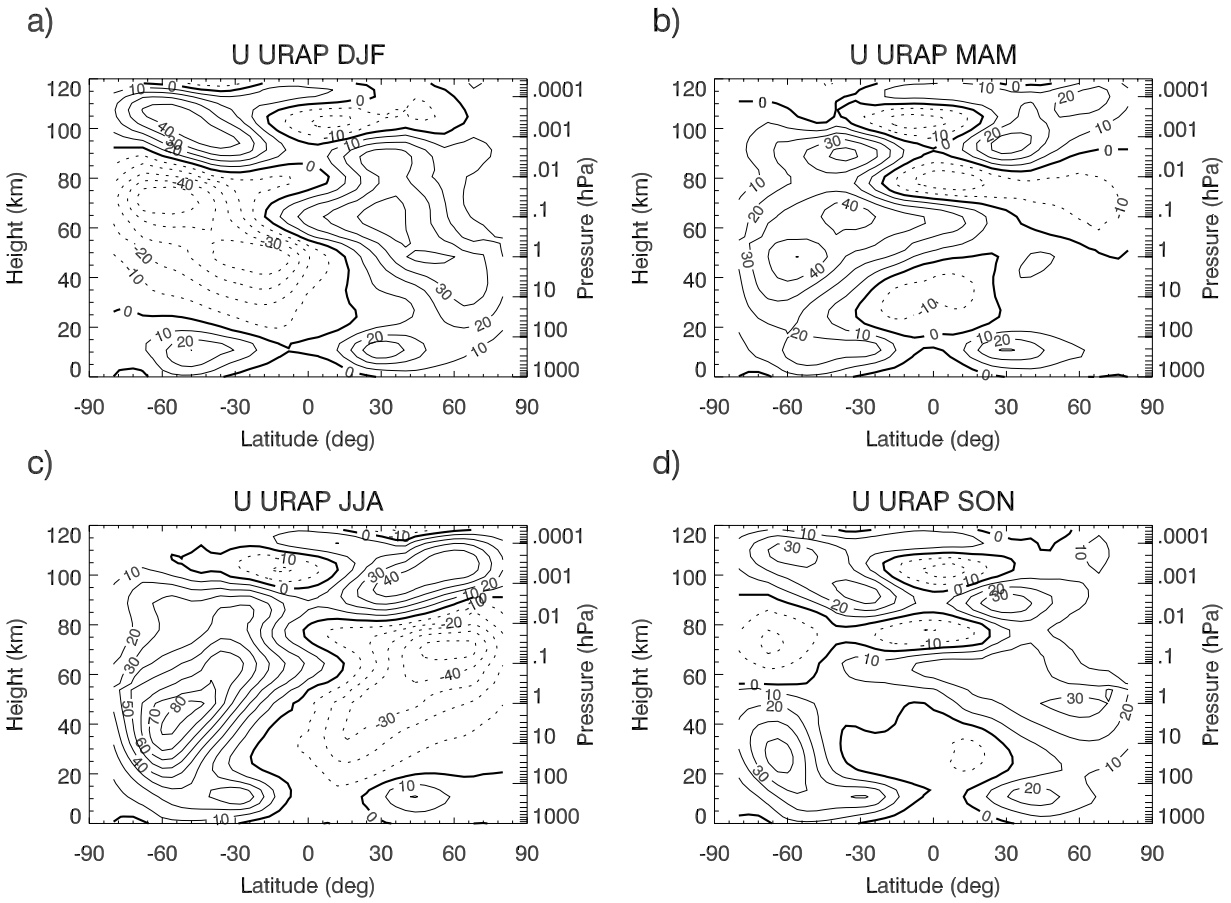

Figure 1. Seasonally averaged URAP zonal wind in m s^{-1}.

spectrum obtained by *Charron and Manzini* [2002] (see *Garcia et al* [2007] for details).

[14] The source mean momentum flux amplitude, τ^*_b, is set to 7×10^{-3} Pa. In order to produce a more realistic model climatology, minor adjustments were made to $F(\phi,t)$, and τ^*_b was set to 6×10^{-3} Pa in the $4^\circ \times 5^\circ$ model.

[15] Note that tuning parameters for two physical parameterizations in CAM3 are also set to different values for the $4^\circ \times 5^\circ$ simulation: the rain water autoconversion coefficient for shallow convection and the cloud fraction threshold for high clouds is different in the $4^\circ \times 5^\circ$ model. These tuning differences are imposed in CAM3 in order to keep the model in energy balance and produce realistic longwave and shortwave cloud forcing. The differences in tuning parameters between different resolutions of WACCM3 imply that middle atmospheric differences in simulations are a combination of differences in forcing and resolution issues. There are no differences in tuning parameters between the $1^\circ \times 1.25^\circ$ and the $1.9^\circ \times 2.5^\circ$ model.

[16] We present here results from 30-year simulations at $1.9^\circ \times 2.5^\circ$ and $4^\circ \times 5^\circ$ and a 5-year simulation at $1^\circ \times 1.25^\circ$. Detailed momentum budgets are calculated from 10 years of 3-h instantaneous model output for the $1.9^\circ \times 2.5^\circ$ and $4^\circ \times 5^\circ$ simulations. Unfortunately, only monthly mean and limited daily data is available for the $1^\circ \times 1.25^\circ$ simulation and hence a detailed momentum budget analysis can not be performed. All simulations are done with climatological mean sea surface temperatures (SSTs), and under solar minimum conditions. The simulations have fully interactive chemistry, with specified chemical boundary values for 1995 (e.g., N_2O, CH_4, CO_2, chlorofluorocarbons and other halogenated compounds) at the surface.

3. Zonal Mean Climatology

[17] Here, we compare WACCM3's zonal mean climatology of zonal winds and temperature to the ERA-40 reanalysis [*Uppala et al.*, 2005] and to the UARS Reference Atmosphere Project (URAP) [*Swinbank and Ortland*, 2003] wind and temperature data. The ERA-40 data set is based mainly on the European Centre's for Medium-Range Weather Forecasts (ECMWF) reanalysis. It covers the period from 1957 to 2000 and extends to 0.1 hPa in altitude. The URAP data set combines observations from the High-Resolution Doppler Imager (HRDI) in the upper stratosphere and MLT with the UK Meteorological Office (UKMO) stratospheric data assimilation system, which provides the data in the troposphere and the lower stratosphere. The seasonal means of the URAP zonal mean wind are shown in Figure 1. In the stratosphere, these winds are very close to those from ERA-40 (not shown). As URAP temperatures (shown in Figure 2) are available only up to 0.1 mbar, for observations of the mesopause temperatures we use 4-year averaged data from the Sounding of the Atmosphere using Broadband Emission Radiometry (SABER) instrument shown in *Xu et al.* [2007].

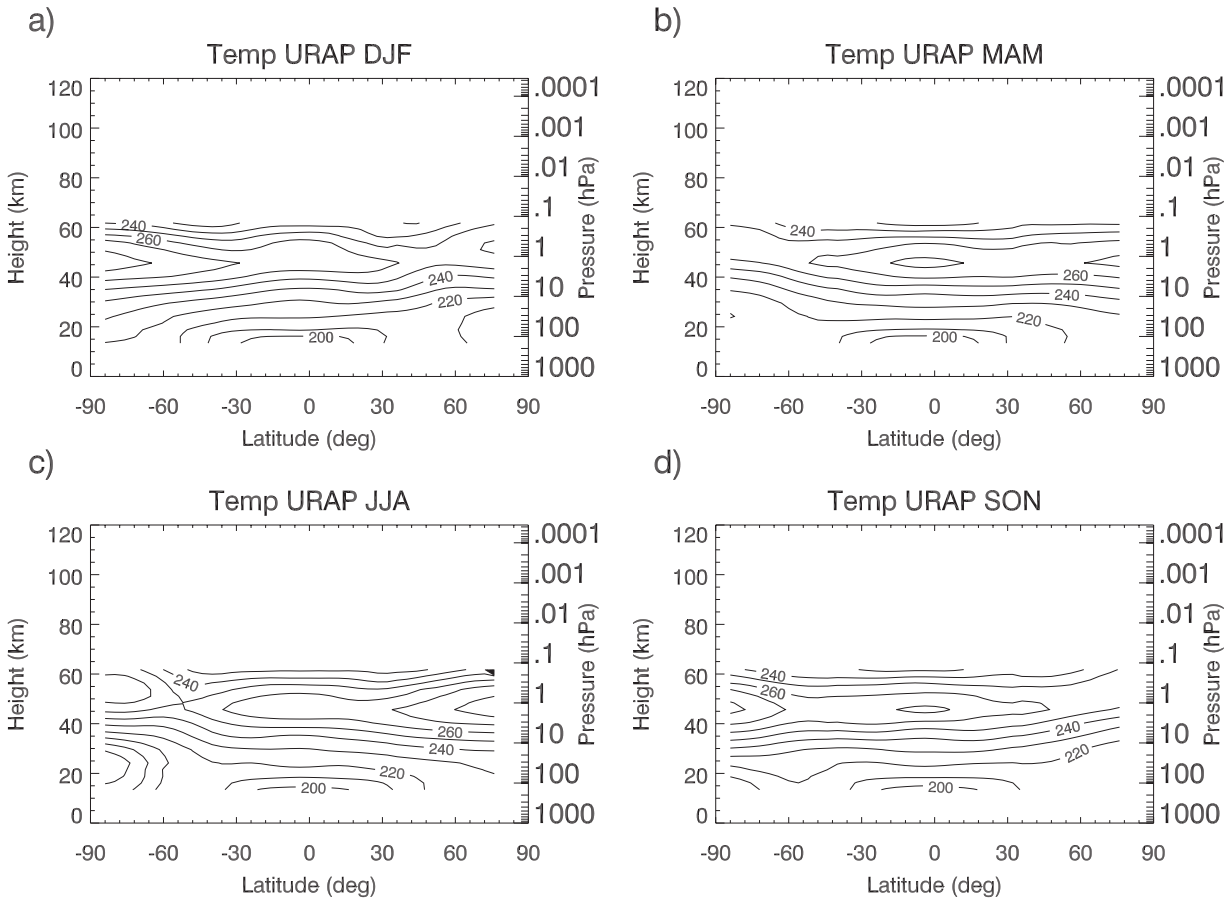

Figure 2. Seasonally averaged URAP temperature degrees Kelvin.

[18] WACCM3 produces a climate that is very similar to that of CAM3 below 100 hPa. Small differences arise from differences in gravity wave parameterization between the two models. For a detailed analysis of the dynamical simulation in WACCM3 in the troposphere, the reader is referred to *Hurrel et al.* [2007].

[19] Figure 3 shows the climatology of the zonal mean wind for the $1.9° \times 2.5°$ WACCM3. The general features of the observed zonal mean wind fields are reproduced by WACCM3. Near the solstices, there are strong jets throughout the stratosphere, and a wind reversal at the mesopause. The strength of the winter stratospheric jets in December, January, and February (DJF) and June, July, August (JJA) in WACCM3 is overestimated by $\sim$10 m s^{-1}. The stratospheric winter jet in JJA does not exhibit an equatorward tilt with height. In DJF, the main difference from observations occurs in the summer tropospheric westerly jet in the Southern Hemisphere, which extends into the lower stratosphere. The strength of the summer stratospheric jets at subtropical latitudes in both DJF and JJA is overestimated by $\sim$20 m s^{-1} in WACCM3. In addition, in DJF the summer jet shows a greater split between subtropical and high latitudes than seen in observations, and in JJA the strongest part of the jet is located in the Tropics (0 to 30 N), rather than near 60 N. The mesospheric winds in WACCM3 near the solstices are in reasonable agreement with observations.

[20] Near the equinoxes, the observed zonal mean winds are generally weaker than near the solstices, with stronger stratospheric winds in the Southern Hemisphere. In both March, April, May (MAM) and September, October, November (SON) WACCM3 overestimates the strength of the westerly jet in the Southern Hemisphere by approximately 20 and 30 m s^{-1}, respectively. The Northern Hemispheric winds in MAM and SON in WACCM3 are in good agreement with observations.

[21] The similarities and differences in the zonal wind between WACCM3 and observations also manifest themselves in the extratropical zonal mean temperature, which is in geostrophic balance with the zonal wind. WACCM3's temperatures in the $1.9° \times 2.5°$ model are shown in Figure 4. In DJF, the upper troposphere and stratosphere near the south pole are too cold but the stratopause temperature itself agrees with URAP (Figure 2). WACCM3's winter stratopause in DJF is 10 K too warm. In JJA, the winter stratopause is 20 K too warm, and the summer stratopause is 10 K too cold. Near the equinoxes the lower stratospheric temperatures in the Southern Hemisphere in WACCM3 are too low, reflecting the differences in the zonal wind field already discussed.

[22] The summer polar mesopause temperatures are near 140 K in both January and July (and about 150 K in a seasonal average, DJF and JJA). Compared to SABER [*Xu et al.*, 2007], the Southern Hemisphere's summer temperatures are in good agreement; however, the Northern Hemisphere's summer temperatures are too warm by 20 K. Although the SABER mesopause temperatures presented

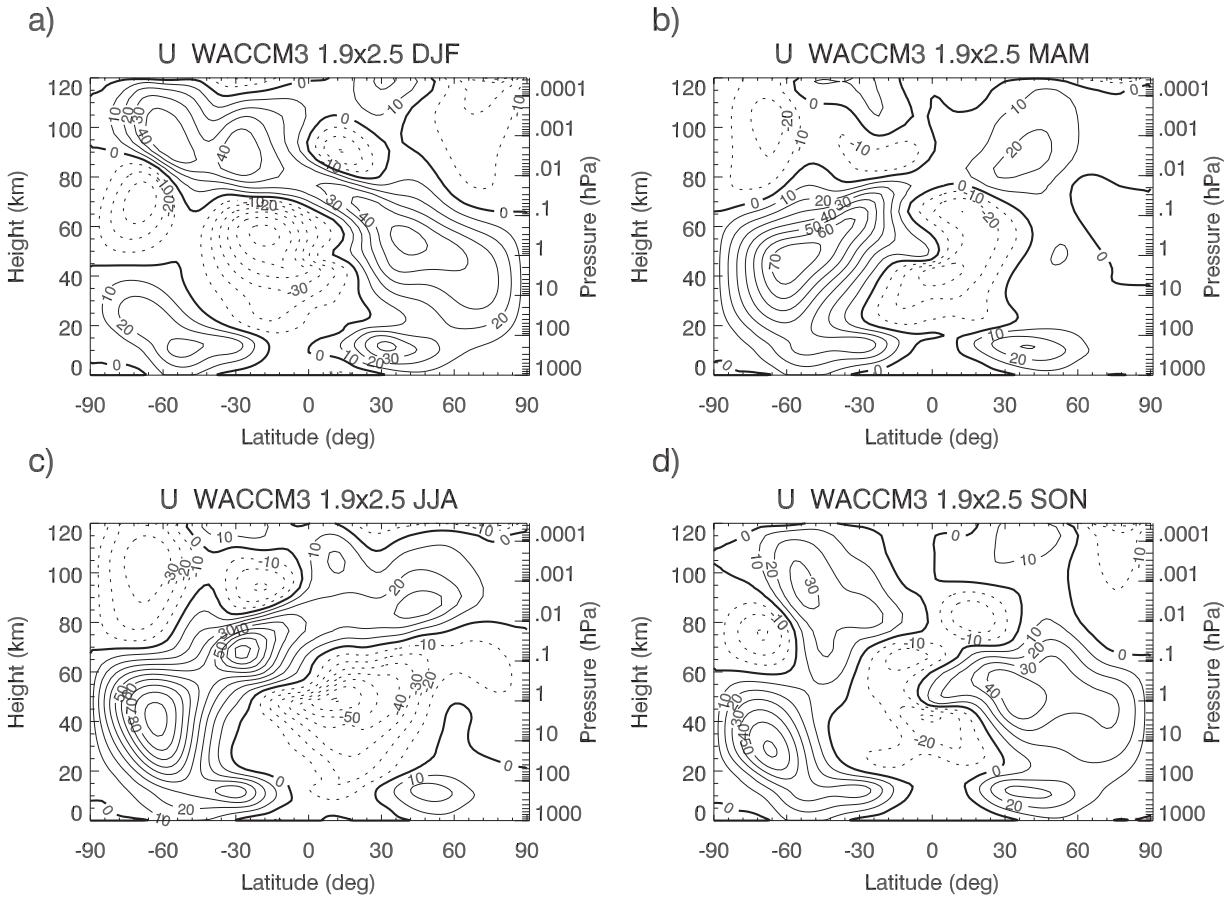

Figure 3. Seasonally averaged zonal wind in m s^{-1} averaged over 30 years of WACCM3 simulation at 1.9° × 2.5° resolution.

by *Xu et al.* [2007] may carry an overall cold bias [*Kutepov et al.*, 2006], the asymmetry between the Northern and Southern Hemisphere's mesopause temperature is a robust feature of this data set, which is not present in WACCM3.

[23] The differences in the zonal mean wind between WACCM3 and observations in the Southern Hemisphere suggest that the momentum budget in this region is not realistic. In particular, it appears that there is missing westward force in the Southern Hemisphere stratosphere. The bias in Southern Hemispheric stratospheric winds in WACCM3 can be improved by changing the configuration of the gravity wave parameterization (not shown); however, the simulation of the mesosphere is then degraded.

[24] The mean middle atmospheric climate in WACCM3 at 4° × 5° and 1 × 1.25° resolution is similar to that at 1.9° × 2.5° resolution. Largest differences between the simulations occur near the mesopause in DJF. This is illustrated in Figure 5. The minimum mesopause temperature is 156.6 K, 149.5 K, and 151.9 K for the 4° × 5°, 1.9° × 2.5°, and 1 × 1.25° models, respectively. The corresponding mesopause heights are 80, 82, and 82.6 km (in log-pressure altitude assuming a scale height of 7 km). Differences in WACCM3 mesopause temperatures at various resolutions are also reflected in the zonal winds. Compared to the 1.9° × 2.5° model, in the 4° × 5° model the mesospheric jet in the summer hemisphere is stronger (Figure 5c), whereas the winds in the MLT region and in the Northern Hemisphere are weaker. In the 1° × 1.25° model largest differences occur in the tropical upper stratosphere and MLT: over 8 K in temperature (Figure 5b) and up to 15 m s^{-1} in wind amplitude (Figure 5a).

[25] It is important to note that there are also significant differences in tropospheric climate in these simulations. The troposphere in the 4° × 5° model is 2 K colder throughout the extratropical troposphere and near the tropical tropopause (Figure 5d). This is largely due to increased water vapor in the upper troposphere in the 4° × 5° model (not shown), which is a consequence of the difference in cloud fraction threshold for high clouds in this model. As parameters in physical parameterizations of tropospheric processes need to be adjusted for different model resolutions, it is not possible to easily separate out the effects of horizontal resolution on tropospheric climate. Hence, differences in middle atmospheric climate can result from three factors: differences in tropospheric forcing (caused by differing climate), the difference in horizontal resolution itself, and differences in the parameterization of gravity waves. We will address the question of which of these factors is primarily responsible for the differences in middle atmospheric climate in the following sections.

[26] While evaluating climate simulations, it is necessary to consider the model's variability at different resolutions in addition to considering the mean state. Hence, we have calculated the standard deviation of zonal wind from monthly

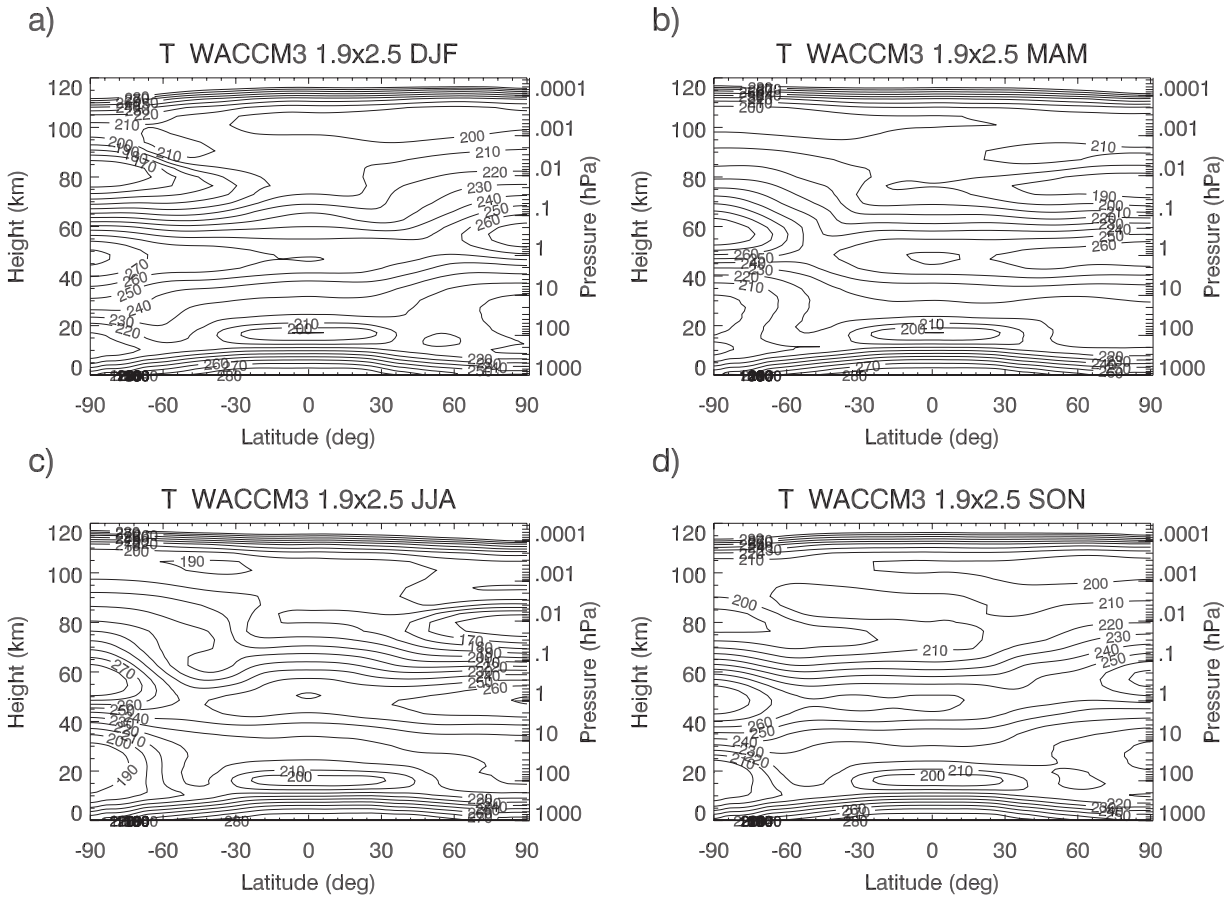

Figure 4. Seasonally averaged temperature in degrees Kelvin averaged over 30 years of WACCM3 simulation at 1.9° × 2.5° resolution.

mean data for the different resolution WACCM3 runs as well as from the ERA-40 reanalysis. This is shown in Figure 6 for DJF. Recall that we only have 5 years available for the 1° × 1.25° simulation, compared to 30 years for the coarser resolution simulations. This analysis shows that the stratospheric variability in winter conditions increases as the model resolution becomes finer: the maximum standard deviation of the zonal wind in the Northern Hemisphere is ~13, 15, and 20 m s^{-1} for the 4° × 5°, 1.9° × 2.5°, and 1° × 1.25° simulation respectively. The increase of stratospheric variability at finer resolution generally occurs during all seasons in WACCM3 (not shown). Small exception occurs in JJA: variability is still lowest in the 4° × 5° model, but highest in the 1.9° × 2.5° model.

[27] In WACCM3 in DJF, most of the variability occurs in the stratosphere between 30 N and 60 N, and there is a secondary maximum near the north pole. This is associated with the interannual variability of the upward propagating quasi-stationary planetary waves. Upward propagating planetary waves deposit momentum to the mean flow in these regions, and hence alter the mean wind and temperature structure. In the mesosphere, the largest variability is also found between 30 N and 60 N; however, it is not significantly different (less than 2 m s^{-1}) among the different resolution simulations.

[28] There are several differences in the standard deviation of the zonal wind in WACCM3 as compared to ERA-40. Firstly, maximum standard deviations in ERA-40 occur in the equatorial lower and middle stratosphere. This is not reproduced in WACCM3, as WACCM3 does not internally generate a quasi-biennial oscillation (QBO). Secondly, the extratropical winter variability in ERA-40 occurs between 60 N and 90 N up to 10 mbar, and moves equatorward above that. The difference in location of maximum variability in WACCM3 from ERA-40 suggests that there are deficiencies in planetary wave propagation in the model. This is likely due to the excessive equatorward extension of the stratospheric westerly jet in WACCM3 as compared to ERA-40.

4. Momentum Budget

[29] In this section we present WACCM3's momentum budget for the different resolution runs. This gives insight into how the mean flow is controlled by the resolved and unresolved features in each case. We examine the momentum budget in WACCM3 by calculating all the forcing terms in the Transformed Eulerian Mean zonal momentum equation [*Andrews et al.*, 1987, p. 128]:

$$\bar{u}_t = -\bar{v}^* \left[(a\cos\phi)^{-1} (\bar{u}\cos\phi)_\phi - f \right] - \bar{w}^* \bar{u}_z - \bar{X} - (\rho_0 a\cos\phi)^{-1} \nabla \cdot \vec{F} \tag{3}$$

where $(\bar{v}^*, \bar{w}^*)$ represent the residual mean meridional circulation, a is the radius of the earth, f is the Coriolis

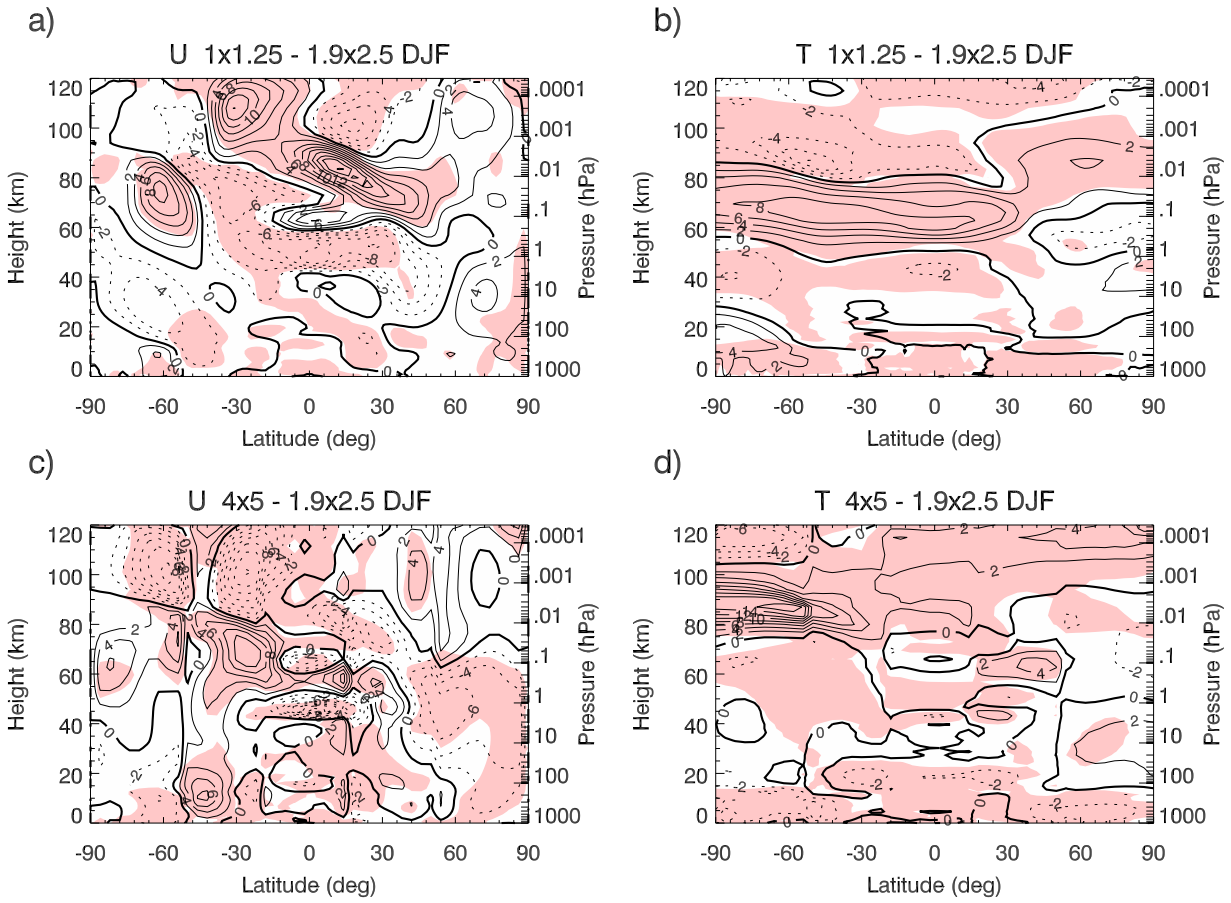

Figure 5. DJF zonal wind and temperature differences (a and b) between WACCM3 simulations at 1° × 1.25° and 1.9° × 2.5° resolution and (c and d) between WACCM3 simulations at 4 × 5° and 1.9° × 2.5° resolution. Shading indicates regions where differences are significant above the 99% confidence level using a Student's *t* test.

parameter, $\bar{X}$ is the drag force from parameterized gravity waves, and $\vec{F}$ is the Eliassen-Palm Flux (EP Flux) due to resolved waves. The first two terms on the right hand side of (3) represent the meridional and vertical advection respectively.

[30] For the 1.9° × 2.5° and 4° × 5° model we use 3-h instantaneous model output from 10 years of simulation to calculate the TEM momentum budget. For the 1° × 1.25° run, the high-frequency model output is not available and hence the budget calculation cannot be performed.

4.1. Stratosphere

[31] Figure 7 shows all the terms in the TEM momentum budget for the 1.9° × 2.5° simulation for DJF and JJA. In the stratosphere, meridional advection is balanced by westward forcing from resolved and parameterized waves. Resolved wave forcing is strongest in the winter hemisphere, and it is about twice as strong in the Southern Hemisphere winter as compared to the Northern Hemisphere winter (4 m s^{-1} d^{-1} vs 2 m s^{-1} d^{-1}). In DJF, there is considerable EP flux divergence from resolved waves in midlatitudes in the summer (Southern Hemisphere) stratosphere. This is due to westerly winds extending up to 40 km in the polar regions, a feature that is not observed. In JJA, stratospheric winds in polar regions are zero or easterly, and hence planetary wave propagation into this region is not possible.

[32] We compare the WACCM3 EP flux divergence due to resolved waves to that derived from stratospheric meteorological analyses from the NOAA Climate Prediction Center (CPC) (see Figure 8). The CPC EP flux divergence is derived from daily data covering altitudes up to ~50 km for the period 1979–2005, based on derived balanced winds [*Randel*, 1987]. The EP flux climatology is described more fully by *Randel* [1992]. The CPC EP fluxes are quite comparable to those derived form the ERA-40 data set (not shown). In order to facilitate the comparison with observations, stratospheric EP flux divergence from WACCM3 is plotted separately in Figure 9, isolating the contribution from waves with horizontal wave numbers 1 and 2. Note that because of the dependence of EP flux divergence on the mean wind itself, comparison of modeled and observed EP flux divergences cannot isolate the cause of discrepancies between modeled and observed climatology. However, such a comparison is still useful as it provides more information on how accurately the model is reproducing the observed features of the middle atmospheric dynamics.

[33] Comparison of Figures 8 and 9 for DJF shows that in Northern Hemisphere winter EP flux divergence due to resolved waves is slightly too small in WACCM3 and does

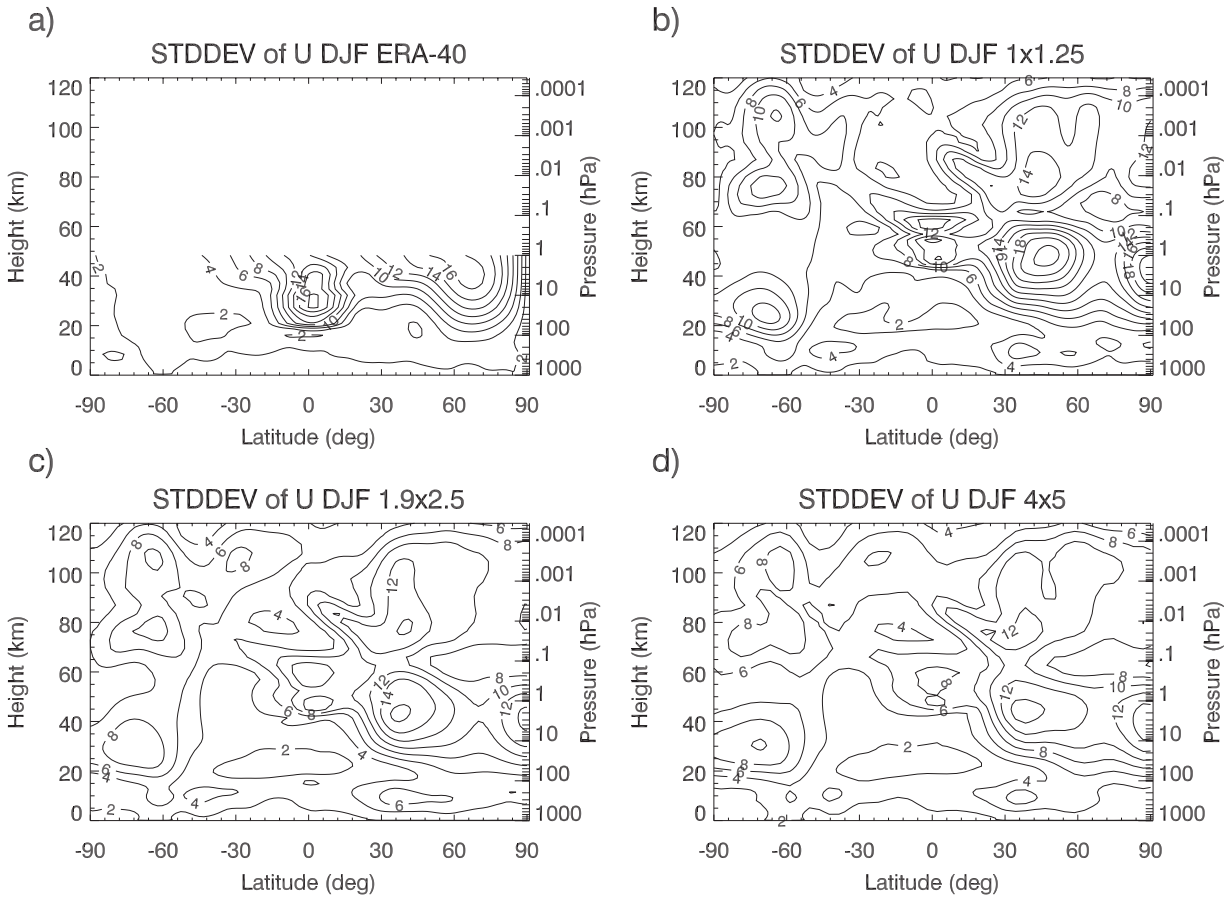

Figure 6. Standard deviation of zonal wind in m s^{-1} for DJF for (a) ERA-40 reanalysis and WACCM3 simulations at (b) 1° × 1.25°, (c) 1.9° × 2.5°, and (d) 4° × 5° resolution.

not occur in the correct location. Observations show EP flux divergences reaching −5 m s^{-1} d^{-1} near 45 km, 35 N; in WACCM3 EP flux divergences in this region only reach −3.5 m s^{-1} d^{-1}. In addition, the local maximum in EP flux divergence near 60 N, ∼38 km in the CPC data is not present in WACCM3. The lack of wave dissipation in this location may be the cause of infrequent occurrence of stratospheric sudden warmings in WACCM3, as will be discussed in section 5.1. In WACCM3 almost all of the resolved wave forcing comes from wave number 1 and 2 waves (compare Figure 9a to Figure 9g). In observations a relatively larger portion of resolved wave forcing comes from waves of higher wave number.

[34] In JJA, the resolved wave forcing in the Southern Hemisphere in WACCM3 is significantly different from observations. Negative EP flux divergences in WACCM3 are three times too large compared to CPC estimates (maximum of 9 m s^{-1} d^{-1} as compared to 3 m s^{-1} d^{-1}). In addition, there is a region of large positive EP flux divergence southward of 70 S. Figures 9d and 9h show that most of the anomalous EP flux divergence in WACCM3 comes from wave number 1. The too strong planetary wave forcing in WACCM3 in JJA is largely due to the jet structure: the westerly stratospheric jet is too strong and has little equatorward tilt compared to observations. This causes a region of instability to form in the polar stratosphere marked by frequent negative values of potential vorticity gradient (not shown). The amplification of wave number 1 wave in this region leads to excessive negative and positive EP flux divergence values.

[35] Parameterized gravity wave drag provides easterly forcing throughout most of the stratosphere during all seasons as shown in Figure 7. It is strongest in DJF and SON in the Northern Hemisphere reaching −7 and −6 m s^{-1} d^{-1} near 1 hPa (∼50 km). Observations of global stratospheric gravity wave drag do not exist; however, *Alexander and Rosenlof* [1996] estimated stratospheric gravity wave drag from National Meteorological Center (NMC) stratospheric analysis and from United Kingdom Meteorological Office (UKMO) assimilated data. These estimates hold a fair degree of uncertainty, especially in the winter season. *Alexander and Rosenlof* [1996] estimate gravity wave drag to be accelerative (in the same direction as the mean wind) throughout the stratosphere above 20 km. This pattern is reproduced by WACCM3 in the summer season, when winds are easterly; however, the amplitude of gravity wave drag is much smaller in WACCM3 as compared to the estimates from NMC and UKMO: In December, at 10 hPa (∼32 km), averaged between 40 S and 70 S, gravity wave drag in WACCM3 is −0.4 m s^{-1} d^{-1}, whereas it is ∼−1 m s^{-1} d^{-1} in both observational estimates. In June, in the extratropics of the summer hemisphere at 10 mbar, gravity wave drag does not exceed 0.1 m s^{-1} d^{-1} in amplitude, whereas it reaches 0.5 m s^{-1} d^{-1} in observations. The fact that gravity wave drag in WACCM3 in the summer stratosphere is smaller than estimated from obser-

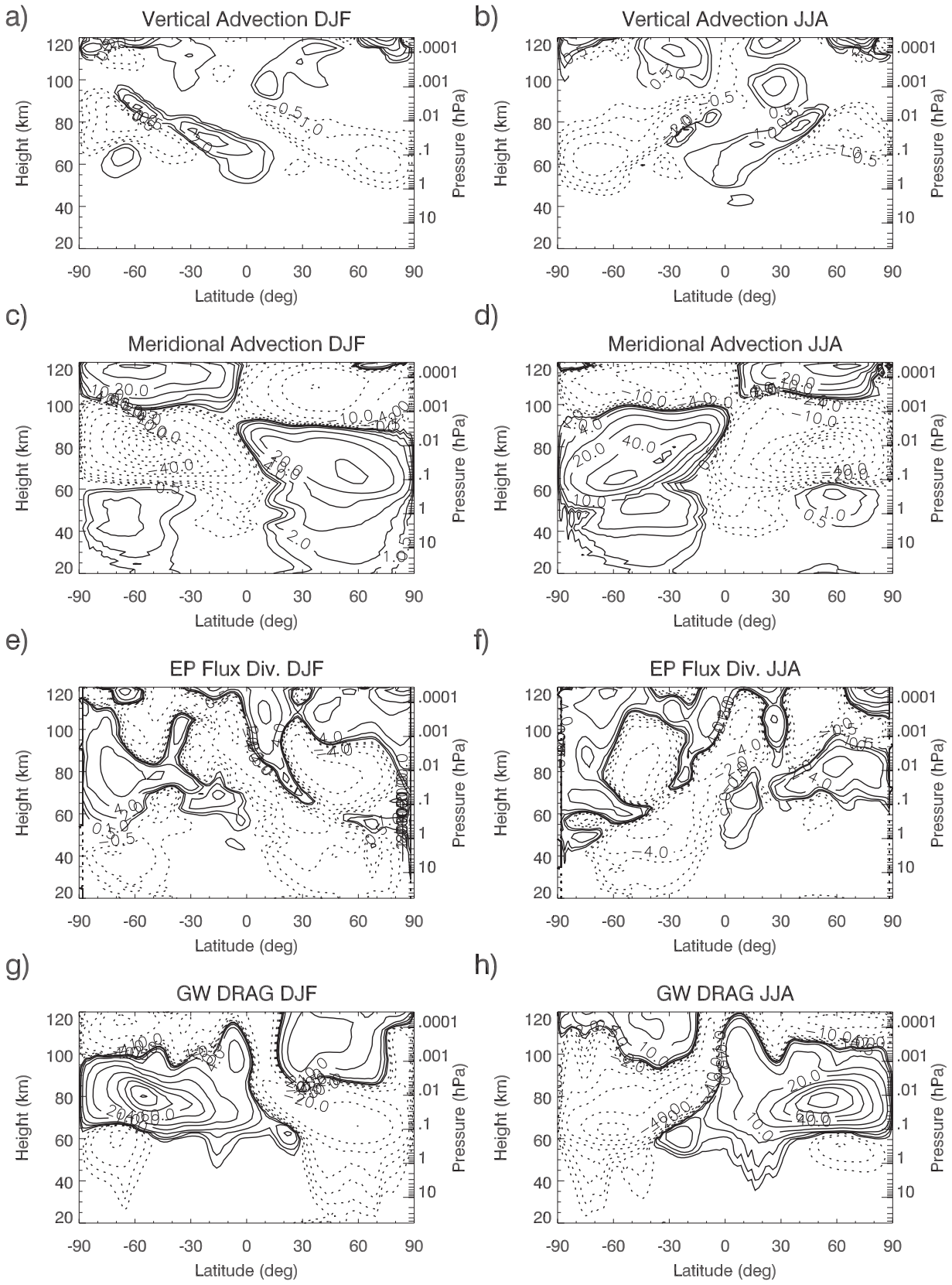

Figure 7. Seasonal mean of vertical advection of zonal momentum, meridional advection of zonal momentum, EP flux divergence, and gravity wave drag for (left) DJF and (right) JJA for 1.9° × 2.5° WACCM3. Contour intervals are ±0.5, ±1, ±2, ±4, ±10, ±20, ±40, ±60, ±80, and ±100 m s^{-1} d^{-1}.

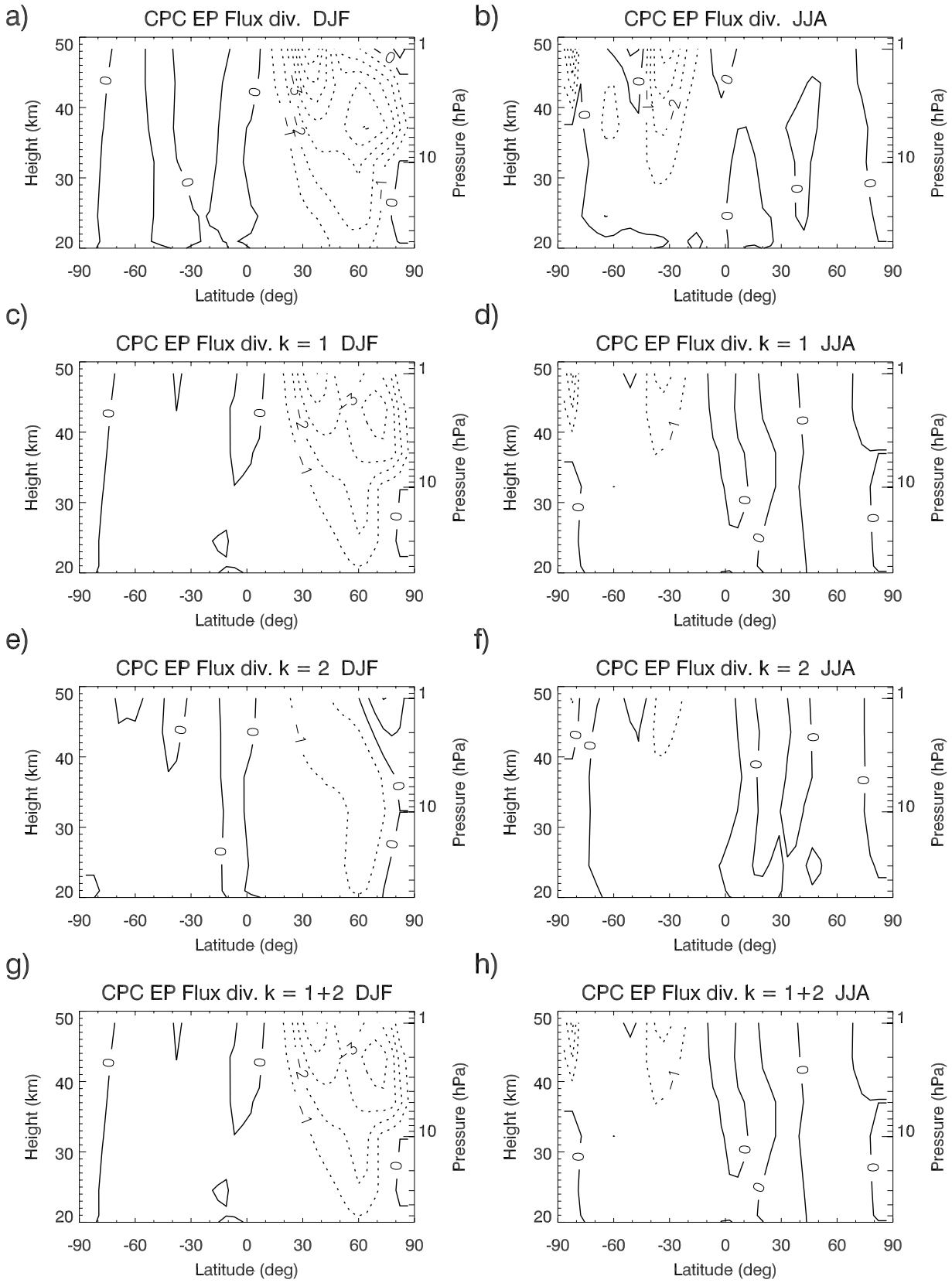

Figure 8. Seasonal mean of EP flux divergence derived from CPC meteorological analyses for (left) DJF and (right) JJA. (a and b) Total EP flux divergence, (c and d) wave number 1 contribution, (e and f) wave number 2 contribution, and (g and h) sum of contributions from wave numbers 1 and 2. Contour interval is 1 m s^{-1} d^{-1}.

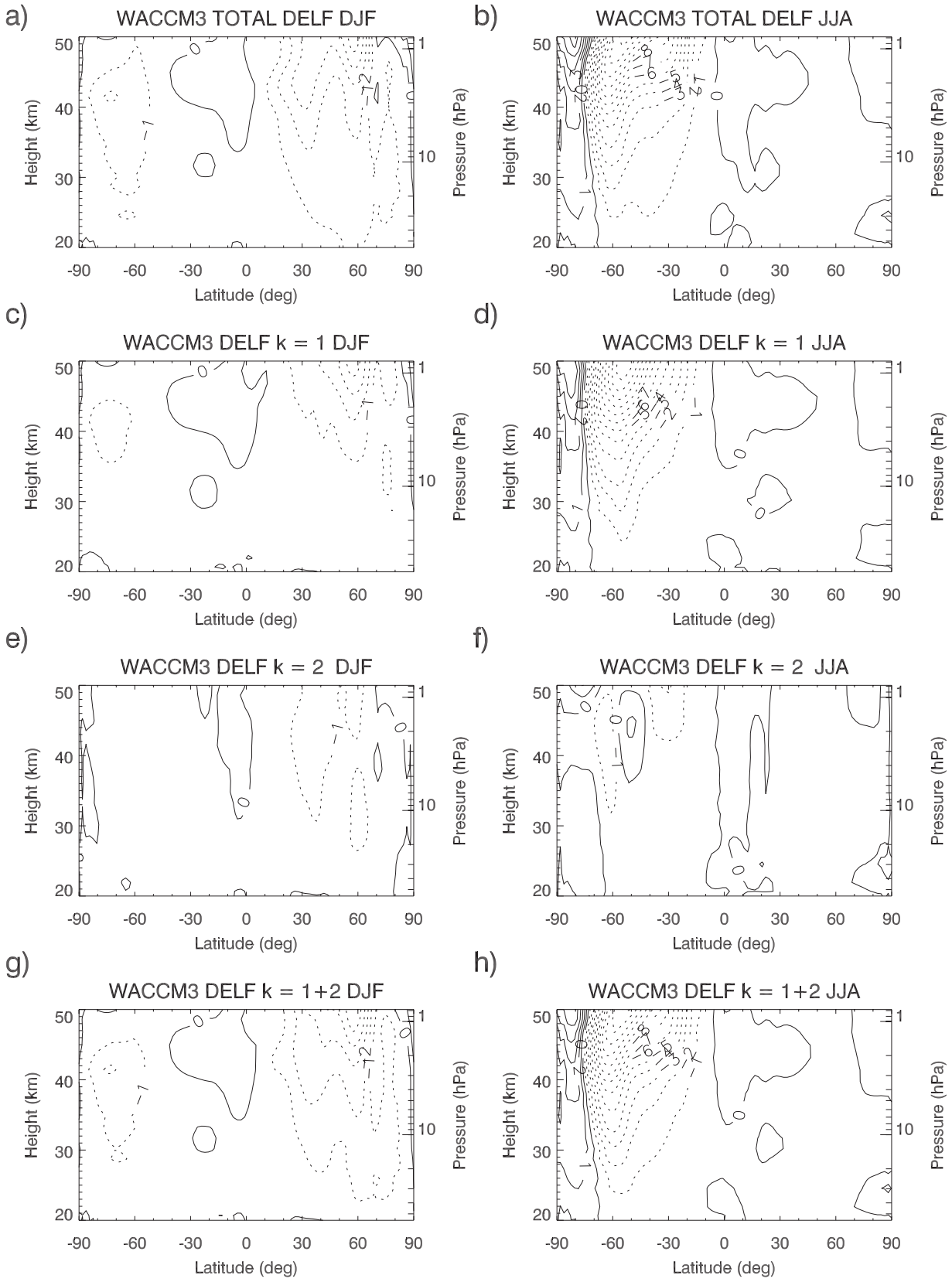

Figure 9. Same as Figure 8 but for WACCM3 at 1.9° × 2.5°.

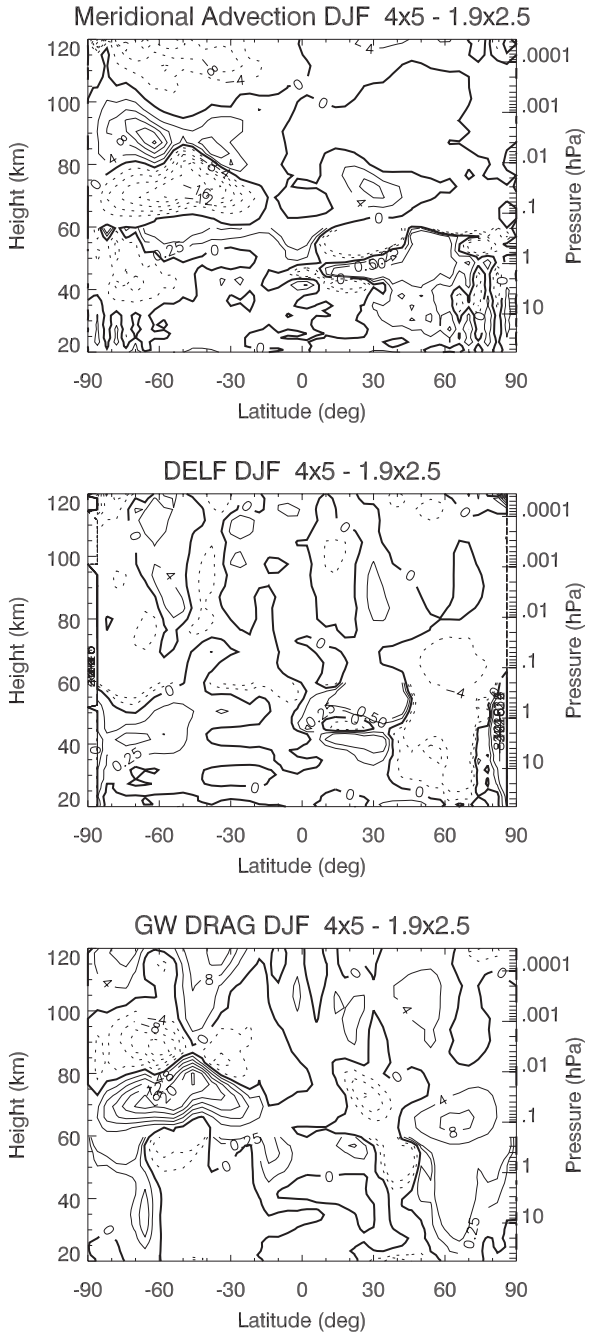

Figure 10. Difference in (top) meridional advection, (middle) EP flux divergence, and (bottom) gravity wave drag between the 4° × 5° and the 1.9° × 2.5° WACCM3 for DJF. Contour interval throughout the domain is 4 m s^{-1} d^{-1}. In addition, the [−0.5, −0.25, 0.25, 0.5] contours are plotted below 60 km.

vations is likely responsible for the extension of the tropospheric westerly jet into the stratosphere in DJF, and weak lower stratospheric polar easterlies in JJA (see Figure 3); however, as gravity wave drag is dependent on the mean wind itself, we cannot rule out that the gravity wave drag is also responding to the mean wind structure. In the winter hemisphere, both in DJF and JJA, the gravity wave drag in WACCM3 acts to decelerate the mean flow. This does not agree with the NMC and UKMO estimates, but as they are uncertain during the winter season, we do not draw any conclusions from this.

[36] The overestimated westerlies in the Southern Hemisphere's summer could potentially be due to too weak easterly drag from planetary waves. A careful examination of tropospheric planetary waves is beyond the scope of this paper, however, we refer the reader to *Hurrel et al.* [2007] for a comparison of planetary waves in CAM3 to ERA-40. This comparison shows that the amplitude of wave number 1 wave at 300 hPa in DJF, in the Southern Hemisphere, is very close to observations. As the winds in CAM3 in the upper troposphere are also quite realistic, it is unlikely that the inaccurate representation of planetary waves in WACCM3 is responsible for the lower stratospheric westerly bias.

[37] The stratospheric momentum budget in the 4° × 5° WACCM3 differs from that in the 1.9° × 2.5° model. This is illustrated in Figure 10 for DJF. The largest differences occur in the winter hemisphere, north of 45 N: as compared to the 1.9° × 2.5° model, the EP flux divergence is ∼25% stronger (more easterly) in the 4° × 5° model, whereas the gravity wave drag is weaker (more westerly) by ∼20% or 0.75 m s^{-1} d^{-1}. The meridional advection in this region is approximately the same. These differences in resolved and parameterized wave forcing result in weaker westerlies throughout the extratropical stratosphere in the 4° × 5° WACCM3 (Figure 5c).

[38] Differences in EP flux divergence between the two resolution models can be due to differences in wave generation and/or differences in wave mean flow interaction. Examination of the 500 hPa geopotential height field (not shown) shows that the planetary wave structure in DJF between the 1.9° × 2.5° and 4° × 5° WACCM3 is very similar; this suggests that differences in stratospheric EP flux divergence result from different wave mean flow interaction due to the use of different gravity wave tuning parameters.

[39] In DJF the momentum budget in the polar Southern Hemisphere in the 4° × 5° WACCM3 is also a little different from the 1.9° × 2.5° model. The meridional advection in the stratosphere becomes more easterly, whereas both the gravity wave drag and EP flux divergence from resolved waves is more westerly.

[40] In JJA (not shown) there are also differences in the momentum budget between the 4° × 5° and 1.9° × 2.5° WACCM3. In JJA EP flux divergences, positive and negative, are 25% weaker in the 4° × 5° model as compared to the 1.9° × 2.5° model, and the gravity wave drag is also weaker. The meridional advection in the extratropical stratosphere at 4° × 5° is less westerly. Unlike in DJF, in JJA, the planetary waves in the troposphere are not the same between the two resolution models: in the 4° × 5° WACCM3, the amplitude of the k = 1 planetary wave is ∼30% larger than in the 1.9° × 2.5° model. As the zonal mean wind in JJA winter is very similar between the models, the differing planetary wave structure in the troposphere is likely the cause of differences in EP flux divergence in the stratosphere.

[41] For the 1° × 1.25°, we can not calculate the entire TEM momentum budget and we are limited to looking at parameterized gravity wave drag. The gravity wave drag in the stratosphere in the 1° × 1.25° WACCM3 is virtually the same as in the 1.9° × 2.5° WACCM3 in DJF (Figure 11). This implies that the differences in the zonal mean wind and

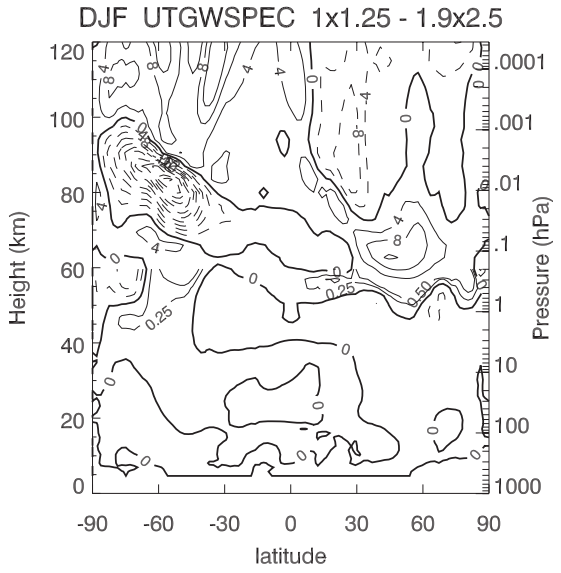

Figure 11. Difference in gravity wave drag between the $1^\circ \times 1.25^\circ$ and the $1.9^\circ \times 2.5^\circ$ WACCM3 for DJF. Contours are the same as in Figure 10.

temperature are caused by resolved dynamical features being represented differently at finer resolutions. In particular, it is most likely that the stationary planetary waves are being forced differently in this version of WACCM3.

4.2. Mesosphere

[42] Figure 7 shows that in the mesosphere and lower thermosphere the main momentum balance is between the meridional advection of zonal momentum and gravity wave drag. These terms are the largest in the summer hemisphere, reaching 100 m s^{-1} d^{-1} in magnitude. Resolved waves also contribute to the budget with amplitudes of no more than 10 to 15 m s^{-1} d^{-1} in a seasonal mean. Vertical advection of zonal momentum is nonnegligible in the mesosphere, reaching magnitudes of 5 m s^{-1} d^{-1} near the summer mesopause. Unfortunately, there are no reliable observations against which we can verify the mesospheric momentum budget. However, we can look at the momentum deposition from individual wave components in the MLT, as these could be compared with observations.

[43] Spectral analysis (not shown) of the EP flux divergence in the MLT shows that there are four wave modes that deposit most momentum in this region. These include the horizontal wave number 1 and 2 quasi-stationary waves, the migrating diurnal tide, and the nonmigrating eastward propagating wave number 3 diurnal tide. Figure 12 shows the EP flux divergence for DJF from these 4 wave components. In JJA the same four wave components dominate (not shown). It is clear from Figure 12 that the stationary waves contribute the largest amount of momentum in the extratropical MLT with the wave number 1 quasi-stationary wave depositing more than 10 m s^{-1} d^{-1} near 70 S, 80 km, and more than -10 m s^{-1} d^{-1} near 70 S, 70 km. Tides are the main contributor of momentum from resolved wave features in the Tropics. The k = 3 nonmigrating diurnal tide contributes almost 10 m s^{-1} d^{-1} near 110 km close to the Equator. The contributions from the migrating diurnal tide are smaller but also sizable. The quasi-2-d wave (described in section 5.2) and the quasi-5-d wave (not shown) also deposit momentum in the MLT, but in a seasonal mean, their momentum deposition is small, less than 2 m s^{-1} d^{-1} in magnitude.

[44] There are considerable differences in the gravity wave drag and meridional advection between the $4^\circ \times 5^\circ$ WACCM3 and the $1.9^\circ \times 2.5^\circ$ WACCM3 (see Figure 10). In the $4^\circ \times 5^\circ$ model, gravity waves break at lower altitudes, increasing the mean flow forcing by over 20 m s^{-1} d^{-1} near 70 km in the Southern Hemisphere extratropics in DJF, and decreasing it by nearly the same amount near 90 km. This causes the wind reversal and the summer mesopause to occur at lower altitude than in the $1.9^\circ \times 2.5^\circ$ WACCM3.

[45] As the mesospheric circulation changes as the result of the changes in gravity wave drag, the meridional advection also differs significantly in the $4^\circ \times 5^\circ$ model. There are also differences in the forcing from resolved waves in the $4^\circ \times 5^\circ$ model as compared to the $1.9^\circ \times 2.5^\circ$ model. These are less than 5 m s^{-1} d^{-1} and come primarily from the k = 1 quasi-stationary wave (not shown), which deposits half as much momentum in the $4^\circ \times 5^\circ$ model as compared to the $1.9^\circ \times 2.5^\circ$ model. Changes in the quasi-stationary planetary wave are likely a consequence of the changes in gravity wave drag and the zonal mean wind; although this wave also acts to alter the wind structure. In JJA, in the summer hemisphere, the differences in momentum budget between the $4^\circ \times 5^\circ$ WACCM3 and the $1.9^\circ \times 2.5^\circ$ WACCM3 are also mainly related to changes in gravity wave drag (not shown). In JJA extratropical eastward gravity wave drag in the $4^\circ \times 5^\circ$ model is over 40 m s^{-1} d^{-1} stronger near 80 km and 20 m s^{-1} d^{-1} weaker near 65 km than in the $1.9^\circ \times 2.5^\circ$ model, causing a colder mesopause.

[46] In the $1^\circ \times 1.25^\circ$ WACCM3, there are also substantial differences in gravity wave drag compared to the $1.9^\circ \times 2.5^\circ$ WACCM3 (see Figure 11). Unfortunately the other terms in the momentum budget are not available for the $1^\circ \times 1.25^\circ$ model. The largest differences in gravity wave drag are also near the summer mesopause. In this case the gravity wave drag in the main breaking region is weaker than in the $1.9^\circ \times 2.5^\circ$ model, resulting in a slightly higher mesopause.

[47] Recall that there are no tuning differences in any of the physical parameterizations between the $1^\circ \times 1.25^\circ$ and the $1.9^\circ \times 2.5^\circ$ WACCM3, and therefore the resulting differences in the MLT climatology must be due to momentum budget differences resulting from model resolution. In the $4^\circ \times 5^\circ$ WACCM3, various parameterizations, including the gravity wave drag parameterization, were tuned to obtain a reasonable climatology. Hence, it does appear that model resolution does have an influence on the dynamics and momentum budget of the MLT, primarily through changed gravity wave drag.

5. Coupling Phenomena

5.1. Sudden Stratospheric Warmings

[48] A sudden stratospheric warming (SSW) is an event where the winter polar stratosphere warms abruptly and the polar vortex slows down or reverses direction. SSWs are initiated by dissipation of upward propagating planetary waves which produce the warming by decelerating the mean flow. The definition of SSWs vary, and here we use

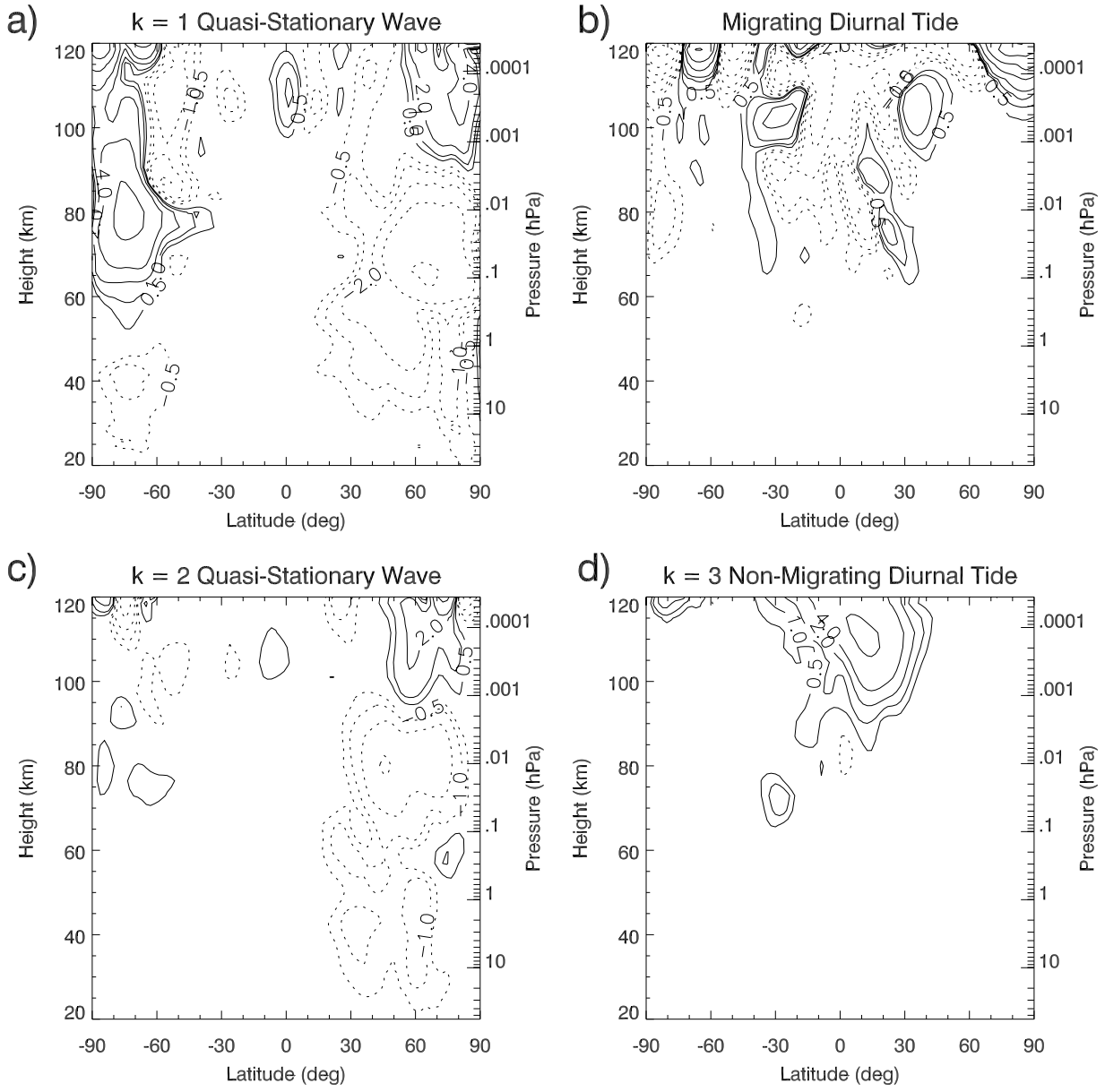

Figure 12. EP Flux divergence from various wave components: (a) k = 1 quasi-stationary wave, (b) migrating diurnal tide, (c) k = 2 quasi-stationary wave, and (d) nonmigrating diurnal tide. Contour interval is the same as in Figure 7.

the official World Meteorological Organization (WMO) [*Labitzke and Naujokat*, 2000] definition to distinguish between midwinter major, final, and minor warmings.We use the following algorithm to automatically calculate the warming statistics for all the simulations:

[49] 1. Major midwinter warming is an event during which the temperature gradient between 60 N and 90 N at 10 hPa is positive for at least 5 d and the zonal mean wind at 60 N at 10 hPa is easterly during that time. If the temperature gradient becomes negative for less than 3 d and then becomes positive again, it is still considered a part of the same warming event.

[50] 2. Minor warming is an event during which the temperature gradient between 60 N and 90 N at 10 hPa is positive for at least 5 d, but there is no reversal of circulation at 10 hPa.

[51] 3. Final warming is a warming event that initiates the transition from winter westerlies to summer easterlies. In other words, the circulation does not return to a winter state after the warming. We consider a warming a final warming when the 21 d running average of the zonal wind at 60 N, 10 hPa does not become positive.

[52] Note, that our definition of a major warming differs from that of *Charlton and Polvani* [2007] who only use the zonal mean wind to diagnose major warmings. As *Charlton and Polvani* [2007] point out, this does not make a big difference to the counts; however, we prefer to use the complete, long-standing WMO definitions. We present the major warmings counts from November through February

Table 1. Frequency of Occurrence of Stratospheric Sudden Warmings: Number of Events and Number of Events per Year in Parentheses

Warming Type	1° × 1.25°	1.9° × 2.5°	4° × 5°	ERA40
Major midwinter (NDJF)	0 (0)	2 (0.1)	3 (0.1)	21 (0.5)
Major midwinter (NDJFM)	1 (0.2)	3 (0.1)	8 (0.3)	25 (0.6)
Major final	0 (0)	0 (0)	0 (0)	12 (0.3)
Minor (NDJF)	4 (0.8)	21 (0.7)	46 (1.5)	39 (0.9)
Minor (NDJFM)	6 (1.2)	43 (1.4)	64 (2.1)	59 (1.4)

(NDJF) and from November through March (NDJFM). We find that separating out the warming events in March elucidates some of the possible reasons for differences between simulated and observed warming frequencies.

[53] We compare the occurrence of SSWs in WACCM3 to that derived from the ERA40 data set for years 1958 to 2000. This is shown in Table 1. Table 1 shows that the frequency of occurrence of major midwinter warmings in WACCM3 is much lower than observed. During NDJF, the frequency of occurrence of major warmings is 0.1, 0.1, and 0 events per year in the 4° × 5°, 1.9° × 2.5°, and 1° × 1.25° model respectively, a fifth or less of the observed frequency of 0.5 events per year. During NDJFM, at all the WACCM resolutions the frequency of occurrence of major warmings increases greatly, especially in the 4° × 5° model (increase from 0.1 to 0.3 events per year). Such a more frequent occurrence of warmings in March relative to NDJF is not observed in ERA-40. In ERA-40 there is only a 20% increase in SSW frequency from NDJF to NDJFM. The presented WACCM3 simulations are forced with climatological and not observed sea surface temperatures and they do not have a quasi-biennial oscillation of the zonal wind (QBO) in the Tropics. These two factors can contribute to, but most likely do not completely explain, the discrepancies between major SSW occurrence between WACCM3 and ERA40. The frequency of SSWs in an older version of WACCM (WACCM1b) and in other GCMs were examined by *Charlton et al.* [2007]. They showed that several of the examined GCMs were deficient in generating SSWs, with WACCM1b producing fewest SSWs. From the study by *Charlton et al.* [2007] it was not clear what were the necessary factors for obtaining reasonable number of SSWs in GCMs.

[54] The frequency of minor warmings in WACCM3 in both NDJF and NDJFM is much closer to observations; it is even greater in the 4° × 5° as compared to ERA40. This is indicative of planetary wave activity reaching the vortex but not being able to break it down. In WACCM3, the winds near the polar stratospheric vortex are very close to observations in a seasonal average (DJF), however in February and March the polar stratospheric winds in the NH, between 10 and 1 hPa are ∼10 m s^{-1} too strong (not shown). Because of these excessively strong polar winds, the deposition of momentum from planetary waves is not sufficient to break down the vortex.

[55] The number of major and minor SSWs is larger in the 4° × 5° WACCM3 simulation as compared to the 1.9° × 2.5° WACCM3 simulation. This is particularly true for major warmings in March: there are 5 major warmings in the 4° × 5° model as compared to 1 in the 1.9° × 2.5° model. The increase of SSWs in the 4° × 5° WACCM3 is likely due to the increased momentum deposition from planetary waves in the polar winter stratosphere during DJF (Figure 10) and March (not shown). Although we only have a 5 year WACCM3 simulation available for analysis at the 1° × 1.25° resolution, the SSW frequency for this simulation (shown in Table 1) is similar to the SSW frequency in the 1.9° × 2.5° model, and the only major warming during the 5 year simulation occurs in March. Therefore, although the 1° × 1.25° WACCM3 exhibits most variability due to planetary wave activity (see Figure 6), this wave activity does not initiate more SSWs. This suggests that the mean climatological state of the model has a greater influence on the SSW occurrence then the model's resolution.

5.2. Two-Day Wave

[56] In this section we examine in more detail the structure of the 2-d wave in WACCM3. We compare this to 2-d wave observations from the Sounding of the Atmosphere using Broadband Emission Radiometry (SABER) instrument on board NASA's Thermosphere Ionosphere Mesosphere Energetics and Dynamics (TIMED) satellite. The data have been processed using a Fourier synoptic mapping (FFSM) algorithm described by *Salby* [1982a, 1982b]. More details on the wave field analysis from SABER are given by *Garcia et al.* [2005]. Figure 13 shows the seasonal cycle of the 2-d wave amplitude (vertical wave number 3) for four different observation years. Figure 13 shows that strong 2-d wave amplitudes are only present near the solstices (late January and late June) near 30–40° latitude in both hemispheres. The 2-d wave as observed by SABER exhibits strong seasonal variability.

[57] In WACCM3 the maximum 2-d wave response is at horizontal wave number 3 and at a frequency of 0.5 cycles d^{-1}, corresponding to a period of exactly 2 d. Figure 14 shows the seasonal cycle of the 2-d wave amplitude averaged over 10 years of simulation. The 10 year average represents well the prominent features of this wave in WACCM3: in the Southern Hemisphere the maximum amplitude occurs very close to the solstice (in late December and early January) and is present mainly between 30 S and 60 S. In the Northern Hemisphere, the 2-d wave occurs about a month before solstice, in late May and early June, for a shorter time period and narrower latitudinal extent centered on 30 N.

[58] Averaged over 10 years the 2-d wave amplitude is quite weak: ∼2 K in the Southern Hemisphere and ∼1.5 K in the Northern Hemisphere. This is in part due to the fact that the 2-d wave amplitude in WACCM3 varies interannually: in 3 out of the 10 analyzed years, its amplitude is negligible. The strongest 2-d wave amplitude in the Southern Hemisphere reaches 4.6 K and 2.4 K in the Northern Hemisphere at 84 km. Observed 2-d wave amplitudes in SABER at this altitude range from ∼3.5–5 K; hence, the 2-d

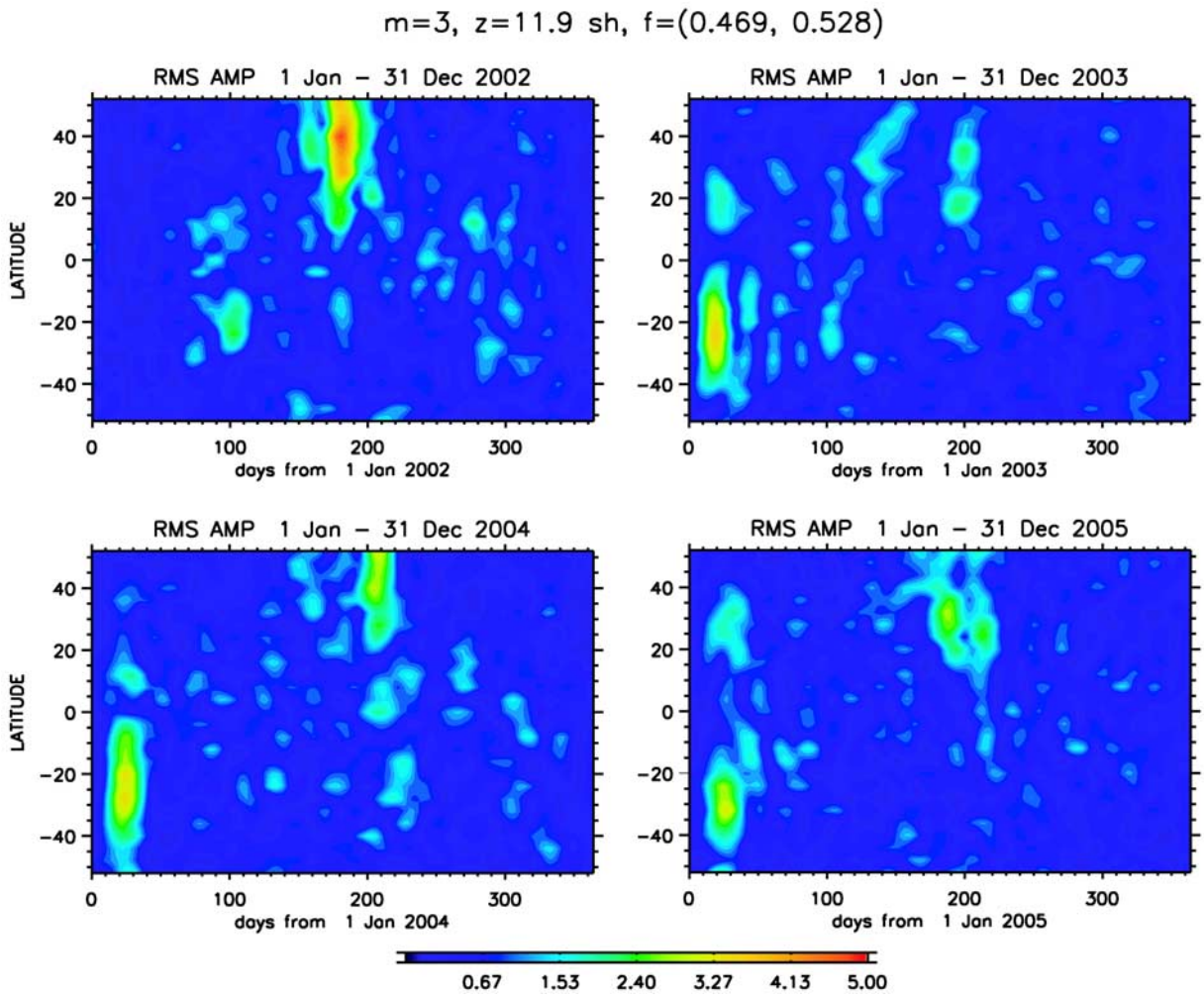

Figure 13. Amplitude of the 2-d wave in degrees Kelvin as a function of time of year and latitude as observed by SABER at 12 scale heights (84 km). The observational year is noted in the top right corner of each panel.

wave in WACCM3 during the strongest event has comparable amplitude as observed; however, in a 10 year mean it is weaker than observed.

[59] Figure 15 shows the height and latitude structure of the 2-d wave amplitude and phase during the strongest event in WACCM3. We compare these to the vertical structure of the 2-d wave as observed by SABER during a January of 2003 event (shown in Figure 16). The structure of the 2-d wave in WACCM3 is in fairly good agreement with observations. Peak amplitude is between 12 and 13 scale heights and near 30 S. Significant wave amplitude can be traced down to 8 scale heights. The wave is present mainly in the Southern Hemisphere but extends to the Northern Hemisphere above 12 scale heights with weaker amplitude both in WACCM3 and observations. The vertical wavelength is very long, ~70 km, in excellent agreement with observations, consistent with its being a normal mode.

[60] The 2-d wave amplifies near solstices by baroclinic instability [*Plumb et al.*, 1982; *Salby and Callaghan*, 2001, 2003]. The latitudinal gradient of potential vorticity and hence the zonal mean wind structure therefore influence the wave amplitude. Figure 17 shows that in WACCM3 near solstice the main region of instability is centered on 65 S and 80 km. The 2-d wave grows in this region as depicted by the EP flux vectors. The reason for the weak amplitude of the 2-d wave in WACCM3 is apparently related to the location of the baroclinic instability region. Because of the split in the easterly stratospheric jet in midlatitudes (continuing from Figure 3), the unstable region is close to the pole; however, in order for a Rossby gravity wave mode to amplify, the instability needs to be located in the subtropics and midlatitudes. This is the case in observations and also occurred in WACCM2 [*Richter and Garcia*, 2006], where the zonal mean wind structure in the SH resembled the observations more closely. This implies that the stratospheric zonal mean wind climatology in global models influences the mesosphere dynamics and momentum budget through the 2-d wave. In WACCM2, the 2-d wave caused accelerations of ~20 m s^{-1} d^{-1} on the mean flow in a monthly mean in the extratropics and ~7 m s^{-1} d^{-1} in the Tropics [*Richter and Garcia*, 2006], whereas in WACCM3 the contribution of the 2-d wave to the momentum budget is only ~2 m s^{-1} d^{-1}.

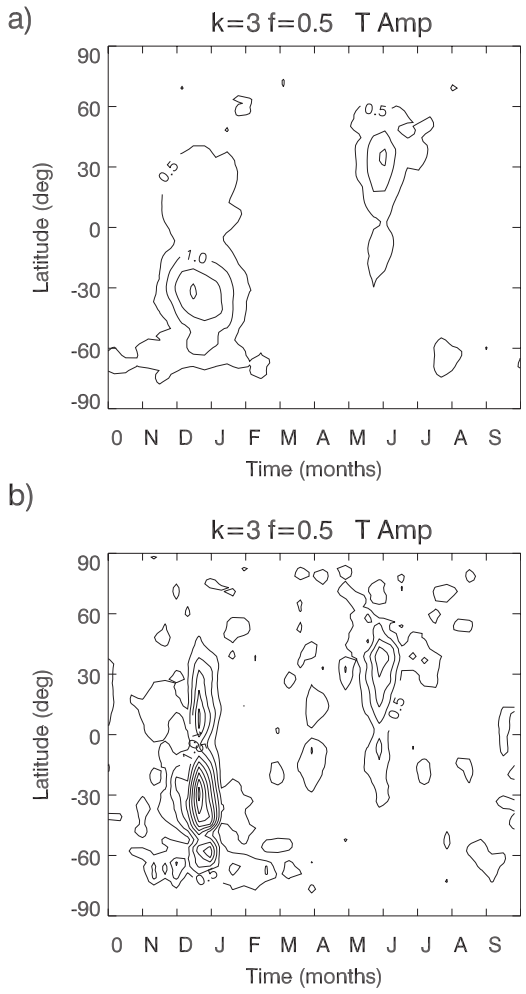

Figure 14. Amplitude of the 2-d wave as a function of time of year and latitude in 1.9° × 2.5° WACCM3 at 84 km (a) averaged over 10 years of simulation and (b) for year with strongest 2-d wave episode. Contour interval is 0.5 K.

[61] The 2-d wave in the 4° × 5° WACCM3 has the same seasonal cycle as in the 1.9° × 2.5° model, with maximum amplitude in late December and late May. However, in the 4° × 5° model, in a 10 year average, the 2-d wave has twice as large amplitude in May in the Northern Hemisphere, over 2.5 K (not shown). This is also true for the individual years. The strongest 2-d wave event in the 4° × 5° model has amplitude of 6.3 K. This is likely due to differences in the zonal mean wind between the two models: in both May and June the westerlies near 30 N between 80 and 100 km are $\sim$10 m s^{-1} stronger in the 4° × 5° model as compared to the 1.9° × 2.5° model (not shown).

5.3. Diurnal Tide

[62] The migrating diurnal tide is the last dynamical feature of the middle atmosphere that we examine in more detail. The migrating diurnal tide is dominant in the MLT region and is driven by the absorption of UV radiation by stratospheric ozone and by latent heating and water vapor shortwave absorption in the troposphere. The migrating diurnal tide is observed to have a semidiurnal variation in amplitude with maxima near the equinoxes. A detailed comparison of the migrating diurnal tide in the 1.9° × 2.5° WACCM3 to the Global Scale Wave Model (GSWM) [*Hagan et al.*, 1995; *Hagan*, 1996] and radar observations are given by *Chang et al.* [2008]. Here we summarize these findings and present a comparison with the 4° × 5° WACCM3.

[63] The general features of the migrating diurnal tide in the 1.9° × 2.5° WACCM3, such as global spatial structure, vertical wavelength, and seasonal amplitude variation, are in general agreement with the GSWM model and previous tidal studies. Compared to the GSWM, WACCM3 exhibits much larger hemispheric asymmetry and significantly smaller amplitudes near equinoxes. The large hemispheric asymmetry in WACCM3 is attributed to the greater complexity of this model as compared to GSWM: GSWM gives a steady state solution to the linearized primitive equations with static background variables such as dissipation and the mean winds, whereas WACCM3 is a fully nonlinear model, with self-consistent dynamics, which allows for feedbacks between tides and the model mean state, as well as allows wave-wave interactions [*Chang et al.*, 2008]. The smaller than observed tidal amplitude at the equinox is believed to be primarily due to considerably lower tropospheric convective heating rates at the diurnal period in WACCM3 as

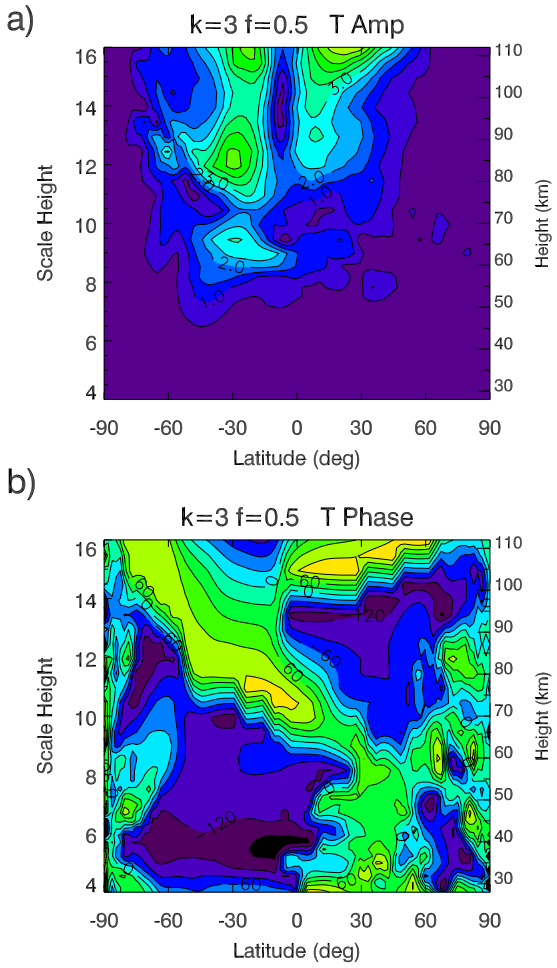

Figure 15. (top) Amplitude in degrees Kelvin and (bottom) phase of the 2-d wave as a function of height and latitude during a strongest wave event in 1.9° × 2.5° WACCM3.

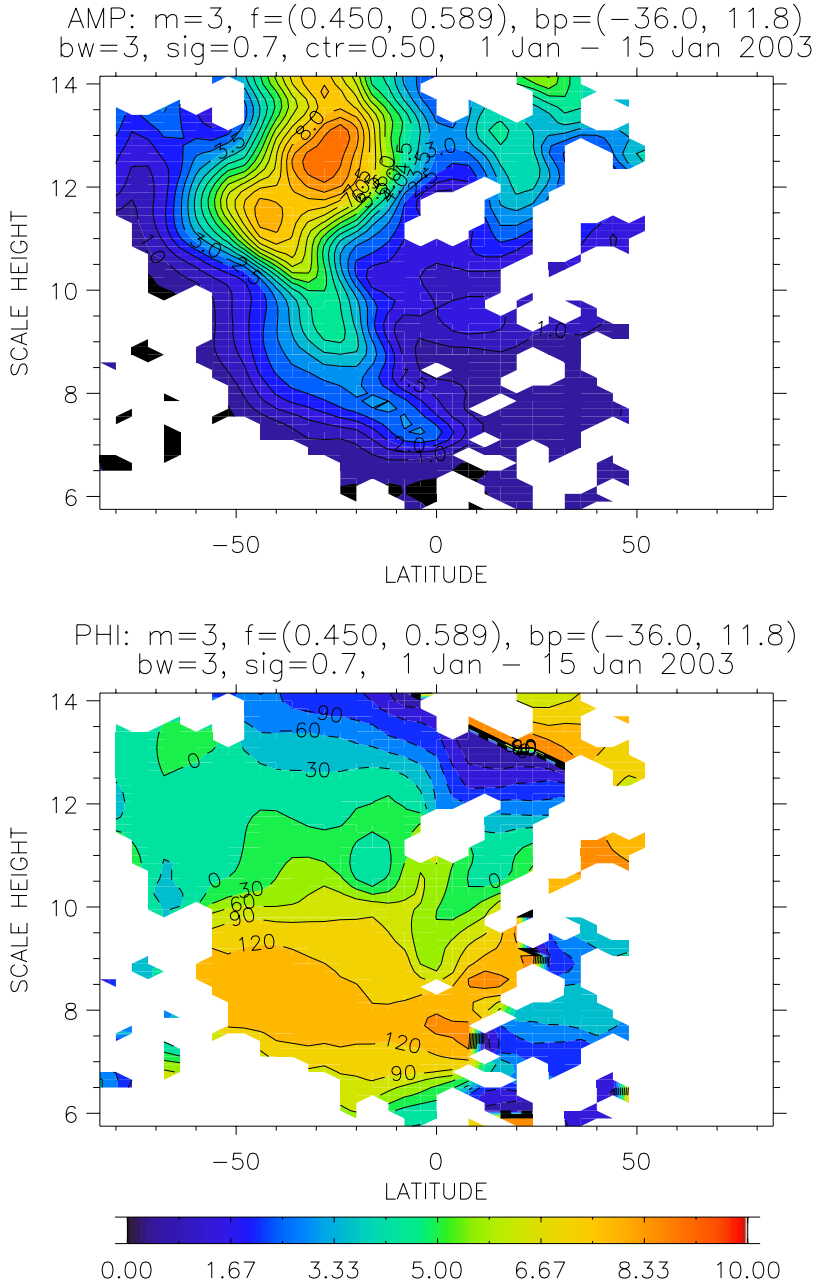

Figure 16. Amplitude in degrees Kelvin and phase of the 2-d wave as observed by SABER in January 2003.

compared to GSWM, as well as due to differences in dissipation and zonal mean wind structure.

[64] Figure 18 shows that the tidal amplitudes in the 4° × 5° WACCM3 are different from those in the 1.9° × 2.5° WACCM3. In the 4° × 5° model amplitudes are higher by 10 m s^{-1} in January in the Southern Hemisphere, and they are lower by nearly 10 m s^{-1} in April in both hemispheres. Detailed examination of the reasons for these discrepancies is beyond the scope of this paper, but horizontal resolution will have a bearing on the amplitude of the migrating diurnal tide, as it has a narrow latitudinal structure. Besides horizontal resolution differences, factors contributing to the amplitude differences of the diurnal tide in the 4° × 5° WACCM3 could include differences in latent heating, dissipation and zonal wind. The phases of the diurnal tide in the 4° × 5° WACCM3 are very close to those in the 1.9° × 2.5° WACCM3 (not shown).

6. Summary and Conclusions

[65] We have presented here a detailed climatology of the dynamical features of the stratosphere, mesosphere and lower thermosphere as represented by the Whole Atmosphere Community Climate Model, version 3 (WACCM3) at various horizontal resolutions (1° × 1.25°, 1.9° × 2.5°, and 4° × 5°). The gross features of the climatology, such as the structure of the stratospheric jets and wind reversals near the mesopause are represented reasonably well at all model resolutions. WACCM3, however, is deficient in representing several finer details of the observed middle atmosphere

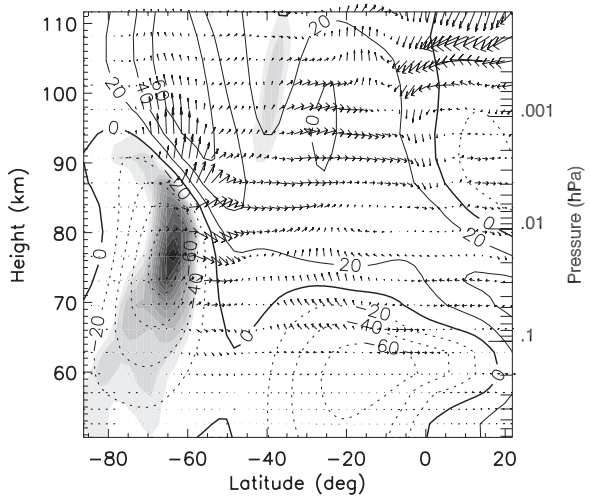

Figure 17. Zonal mean wind (contoured), EP flux vectors, and potential vorticity gradient (shaded) during a strongest wave event in 1.9° × 2.5° WACCM3. Contour interval for the zonal wind is 10 m s^{-1}. Only negative values of potential vorticity are shaded in the following intervals: [−1.95, −1.8, −1.65, −1.5, −1.35, −1.2, −1.05] × 10^{-10}, [−9.0,−7.5, −6.0, −4.5, −3.0] × 10^{-11} m^2 s^{-1} K kg^{-1}.

climatology: (1) in DJF, the tropospheric westerly jet in the Southern Hemisphere extends into the stratosphere; (2) the summer stratospheric easterly jet is split more strongly in midlatitudes than observed; and (3) the winter stratospheric jet in the Southern Hemisphere does not exhibit and equatorward tilt with height. These deficiencies in the zonal mean wind field also manifest themselves in the temperature field: (1) in DJF, the upper troposphere and lower stratosphere is too cold near the south pole; (2) the winter stratopause in both DJF and JJA is too warm; and (3) the JJA summer mesopause is too warm.

[66] In order to obtain further insight into the dynamics of the middle and upper atmosphere in WACCM3, we have performed an analysis of the momentum budget. In the stratosphere, meridional advection is balanced by westward forcing from resolved and parameterized waves in the winter season. In the summer stratosphere, gravity wave drag from parameterized waves is the dominant term opposing meridional advection. In the summer stratosphere, differences in zonal mean wind and temperature structure in WACCM3 from observations must be due to the inappropriate representation of unresolved gravity waves. This is likely the case in DJF in the Southern Hemisphere, where the tropospheric westerly jet in WACCM3 extends into the lower polar stratosphere, suggesting that the gravity wave drag is notsufficiently easterly in this region.

[67] During the winter season, forcing from resolved and parameterized waves are tightly coupled to each other and to the zonal mean wind structure; hence, it is impossible to say with certainty what is the cause and what is the effect of the deficient climatology. However, comparison of WACCM3's EP flux divergences to observations is still useful, as it is another diagnostic of how realistically WACCM3 represents stratospheric dynamics. In WACCM3, the EP flux divergence is weaker compared to CPC estimates by 1.5 m s^{-1} d^{-1} in DJF near 45 km (35 N) and only comes from waves with horizontal wave number 1 and 2. In JJA the EP flux divergence in WACCM3 is too large and there is a region of positive EP flux divergence in the polar region that is not observed.

[68] In the MLT there are no observations that we can compare to WACCM's momentum budget; however, as gravity waves are the dominant term, their inaccurate representation is a likely cause of the differences between WACCM3's and URAP's temperature and wind climatology.

[69] The momentum budget, and hence the zonal wind and temperature climatology, in WACCM3's stratosphere and mesosphere are sensitive to the model's resolution. For example, In DJF, in the extratropical winter stratosphere, the EP flux divergence from resolved waves is ∼25% stronger, and gravity wave drag is ∼20% weaker in the 4° × 5° model as compared to the 1.9° × 2.5° model. In the mesosphere, the main differences in momentum budget between the 4° × 5° and 1.9° × 2.5° model come from differences in gravity wave drag. These changes, however, impact the resolved wave field quite strongly. For example, the quasi-stationary wave deposits half as much momentum in the MLT in the 4° × 5° model as compared to the 1.9° × 2.5°. Recall that in the 4° × 5° model the gravity wave parameterization has slightly different tuning; hence, we can not say with certainty that the resolved dynamics differ only because of the model resolution, but the differences in the wave mean flow interaction between these two resolution models may be important for carrying out scientific studies with WACCM3. In the MLT, zonal mean winds and temperatures are similar between WACCM3 at different horizontal resolutions, but the details of the MLT wave dynamics differ vastly.

[70] The 1° × 1.25° WACCM3 has no differences in physical parameterizations from the 1.9° × 2.5° WACCM3. In the stratosphere, the parameterized gravity wave drag in the 1° × 1.25° WACCM3 is virtually the same as in the 1.9° × 2.5° WACCM3 and stratospheric wind and temperature differences are small and mainly insignificant. In the MLT, large differences in gravity wave drag, zonal wind and temperature in these two models occur near the summer mesopause, suggesting that resolved wave features are indeed sensitive to model's resolution in the MLT.

[71] In this paper we have also examined in detail three coupling processes between the lower and upper atmosphere: stratospheric sudden warmings (SSWs), the 2-d wave, and the migrating diurnal tide. The SSW frequency in WACCM3 is significantly lower than observed (see Table 1). In November through February, the frequency of major midwinter warmings is 0.1 events per year, or one fifth of that observed. In the 4° × 5° WACCM3 the frequency of occurrence of major midwinter warmings increases in March, due to weakened westerlies. The 2-d wave in WACCM3 has close to the observed period; however, it is generally weaker in amplitude, reaching only 2 K in a 10 year simulation average. The weak 2-d wave amplitude is attributed to the structure of the stratospheric summer jet. The migrating diurnal tide in WACCM3 has a spatial structure, vertical wavelength and seasonal amplitude variation in general agreement with observations. Its amplitude at equinoxes is weaker than observed and this is mainly due to lower than observed latent heating rates as described by *Chang et al.* [2008].

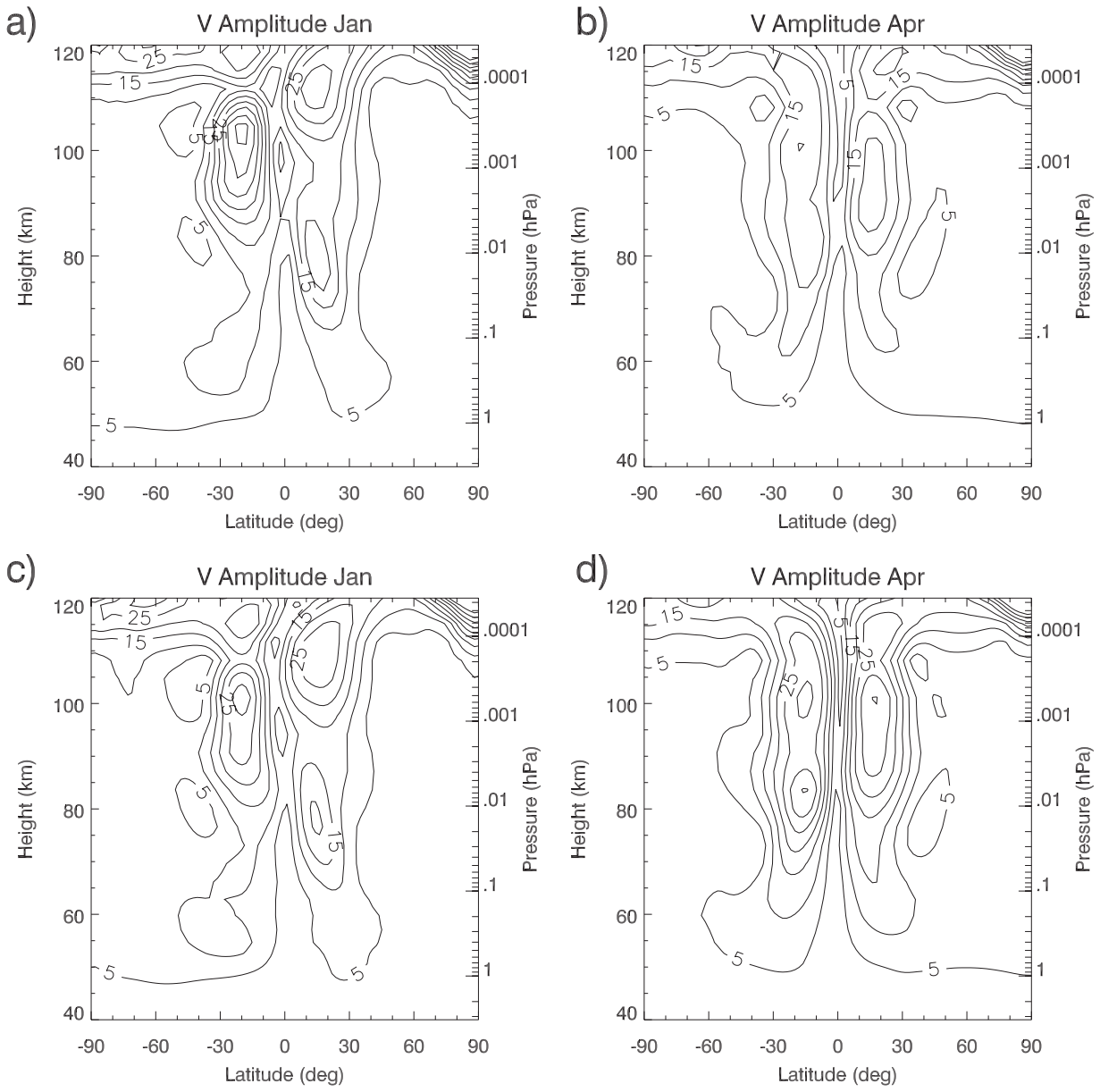

Figure 18. Migrating diurnal tide amplitude for meridional wind for (left) January and (right) April for the (top) 4° ×5° and (bottom) 1.9° × 2.5° WACCM3 simulation. Contour interval is 5 m s^{-1}.

[72] The coupling processes between the lower and upper atmosphere, in particular the sudden stratospheric warmings and the 2-d wave, have shown high sensitivity to the middle atmospheric dynamics and they differ among the different resolution models. The SSW frequency is largest in the 4° × 5° WACCM3, most likely due to increased planetary wave momentum deposition in the polar winter stratosphere. Although we found that the variability increases as the model's resolution become finer, this does not cause more warming events: the 1° × 1.25° WACCM3 has the same low frequency of warmings as the 1.9° × 2.5° WACCM3.

[73] The 2-d wave in the 4° × 5° WACCM3 has the same dominant period, wave number, and seasonal cycle as in the 1.9° × 2.5° WACCM3; however, its amplitude in May in the Northern Hemisphere is nearly twice as large as in the 1.9° × 2.5° WACCM3. This suggests that changes in the zonal winds of order of 10 m s^{-1} can have a large effect on this wave feature and on the momentum budget of the MLT near solstices. The migrating diurnal tide has also different amplitude in the 4° × 5° WACCM3 as compared to the 1.9° × 2.5° WACCM3. Because of the numerous factors that can affect the migrating diurnal tide, such as forcing, stratospheric winds, dissipation, we are unable to determine conclusively why these differences occur.

[74] When pursuing a scientific study with a high-top GCM such as WACCM3, the model's horizontal resolution must be chosen. This study suggests that the choice of horizontal resolution may depend on the particular study or application. This current study with WACCM3 shows that although variability in the stratosphere increases with increased model resolution, this does not improve the representation of the mean wind or temperature in this region. The stratospheric sudden warming frequency is actually more realistic in the coarser resolution model. In the

stratosphere the dominant wave features are of horizontal wave number 1 and 2 and are represented well even at 4° × 5°, hence for scientific studies focusing on this region, this resolution may be enough. On the other hand, in the mesosphere, dynamical features such as the migrating diurnal tide have smaller latitudinal extent and need finer resolution for their accurate representation. Hence, if one is interested in the dynamical features of the MLT, resolution of 1.9° × 2.5° or finer is desired. However, regardless of what horizontal resolution is chosen, in this study we have found that the representation of parameterized gravity waves is what really determines how well the model reproduces the observed dynamical mean state. We have also found, that the mean climatological state of the model has greater influence than the model's resolution on the lower and upper atmospheric coupling processes, such as stratospheric sudden warmings and the 2-d wave.

[75] **Acknowledgments.** We thank William Randel for providing the CPC EP flux divergence analysis. The National Center for Atmospheric Research is sponsored by the National Science Foundation. This work was partly supported by NASA grant MAP/04-0000-047.

References

Alexander, M. J., and K. H. Rosenlof (1996), Nonstationary gravity wave forcing of the stratospheric zonal mean wind, *J. Geophys. Res.*, *101*(D18), 23,465–23,474.

Andrews, D. G., J. R. Holton, and C. B. Leovy (1987), *Middle Atmosphere Dynamics*, Elsevier, New York.

Baldwin, M. P., and T. J. Dunkerton (1999), Propagation of the Arctic Oscillation from the stratosphere to the troposphere, *J. Geophys. Res.*, *104*, 30,937–30,946.

Boville, B. A. (1984), The influence of the polar night jet on the tropospheric circulation in a GCM, *J. Atmos. Sci.*, *41*, 1132–1142.

Chang, L., S. Palo, M. Hagan, J. Richter, R. Garcia, D. Riggin, and D. Fritts (2008), Structure of the migrating diurnal tide in the Whole Atmosphere Community Climate Model (WACCM), *Adv. Space Res.*, in press.

Charlton, A. J., and L. M. Polvani (2007), A new look at stratospheric sudden warming events: Part I. Climatology and modelling benchmarks, *J. Clim.*, *20*, 449–469.

Charlton, A. J., et al. (2007), A new look at stratospheric sudden warming events: Part II. Evaluation of numerical model simulations, *J. Clim.*, *20*, 470–488.

Charron, M., and E. Manzini (2002), Gravity waves from fronts: Parameterization and middle atmosphere response in a General Circulation Model, *J. Atmos. Sci.*, *59*, 923–941.

Collins, W. D., et al. (2006), The formulation and atmospheric simulation of the Community Atmosphere Model: CAM3, *J. Clim.*, *19*, 2144–2161.

Dunkerton, M. P. B. T. J. (2001), Stratospheric harbingers of anomalous weather regimes, *Science*, *294*, 581–584.

Fomichev, V. I., W. E. Ward, S. R. Beagley, C. McLandress, J. C. McConnell, N. A. McFarlane, and T. G. Shepherd (2002), Extended Canadian Middle Atmosphere Model: Zonal-mean climatology and physical parameterizations, *J. Geophys. Res.*, *107*(D10), 4087, doi:10.1029/2001JD000479.

Garcia, R. R., et al. (2005), Large-scale waves in the mesosphere and lower thermosphere observed by SABER, *J. Atmos. Sci.*, *62*, 4384–4399.

Garcia, R. R., D. R. Marsh, D. E. Kinnison, B. A. Boville, and F. Sassi (2007), Simulation of secular trends in the middle atmosphere, 1950–2003, *J. Geophys. Res.*, *112*, D09301, doi:10.1029/2006JD007485.

Hagan, M. E. (1996), Comparative effects of migrating solar sources on tidal signatures in the middle and upper atmosphere, *J. Geophys. Res.*, *101*, 21213–21222.

Hagan, M. E., J. M. Forbes, and F. Vial (1995), On modeling migrating solar tides, *J. Geophys. Res.*, *100*, 893–896.

Hurrel, J. W., et al. (2007), The dynamical simulation of the Community Atmosphere Model version 3 (CAM3), *J. Clim.*, *19*, 2162–2183.

Jablonowski, C., and D. L. Williamson (2006), A baroclinic instability test case for atmospheric model dynamical cores, *Q.J.R. Meteorol. Soc.*, *132*, 2943–2975.

Kutepov, A. A., A. G. Feofilov, B. T. Marshall, L. L. Gordley, W. D. Pesnell, R. A. Goldberg, and J. M. Russell III (2006), SABER temperature observations in the summer polar mesosphere and lower thermosphere: Importance of accounting for the CO2 ?2 quanta V-V exchange, *Geophys. Res. Lett.*, *33*, L21809, doi:10.1029/2006GL026591.

Labitzke, K., and B. Naujokat (2000), The lower Arctic stratosphere in winter since 1952, *SPARC Newsl.*, *15*, 11–14.

Lieberman, R. S. (2002), Corrigendums, *J. Atmos. Sci.*, *59*, 2625–2627.

Lieberman, R. S., and P. B. Hays (1994), An estimate of the mometum deposition in the lower thermosphere by the observed diurinal tide, *J. Atmos. Sci.*, *51*, 3094–3105.

Lin, S. J. (2004), A "vertically Lagrangian" finite-volume dynamical core for global atmospheric models, *Mon. Weather Rev.*, *132*, 2293–2307.

Lindzen, R. S. (1981), Turbulence and stress owing to gravity wave and tidal breakdown, *J. Geophys. Res.*, *86*(C10), 9707–9714.

Marsh, D. R., R. R. Garcia, D. E. Kinnison, B. A. Boville, F. Sassi, S. C. Solomon, and K. Matthes (2007), Modeling the whole atmosphere response to solar cycle changes in radiative and geomagnetic forcing, *J. Geophys. Res.*, *112*, D23306, doi:10.1029/2006JD008306.

McFarlane, N. A. (1987), The effect of orographically excited wave drag on the general circulation of the lower stratosphere and troposphere, *J. Atmos. Sci.*, *44*, 1775–1800.

Norton, W. A., and J. Thuburn (1996), The two-day wave in a middle atmosphere GCM, *Geophys. Res. Lett.*, *23*, 2113–2116.

Plumb, R. A., R. A. Vincent, and R. L. Craig (1982), The quasi-two day wave event of January 1984 and its impacts on the mean mesospheric circulation, *Aust. Meteorol. Mag.*, *30*, 107–121.

Polvani, L. M., and D. W. Waugh (2004), Upward wave activity flux as precursor to extreme stratospheric events and subsequent weather regimes, *J. Clim.*, *17*, 3548–3554.

Randel, W. J. (1987), The evaluation of winds from geopotential height data in the stratosphere, *J. Atmos. Sci.*, *44*, 3097–3120.

Randel, W. J. (1992), Global atmospheric circulation statistics,1000-1 mb, *NCAR Tech. Note, NCAR/TN-366+STR*, 256 pp. Natl. Cent. for Atmos. Res., Boulder, Colo.

Richter, J. H., and R. R. Garcia (2006), On the forcing of the Mesospheric Semi-Annual Oscillation in the Whole Atmosphere Community Climate Model, *Geophys. Res. Lett.*, *33*, L01806, doi:10.1029/2005GL024378.

Salby, M. L. (1981), The 2-day wave in the middle atmosphere: Observations and theory, *J. Geophys. Res.*, *86*, 9654–9660.

Salby, M. L. (1982a), Sampling theory for asynoptic satellite observations. Part I: Space-time spectra, resolution, and aliasing, *J. Atmos. Sci.*, *39*, 2577–2600.

Salby, M. L. (1982b), Sampling theory for asynoptic satellite observations. Part II: Fast Fourier synoptic mapping, *J. Atmos. Sci.*, *39*, 2601–2614.

Salby, M. L., and P. F. Callaghan (2001), Seasonal amplification of the 2-day wave: Relationship between normal mode and instability, *J. Atmos. Sci.*, *58*, 1858–1869.

Salby, M. L., and P. F. Callaghan (2003), Dynamics of the 2-day wave in a nonlinear model of the middle and upper atmosphere, *J. Geophys. Res.*, *108*(D23), 4713, doi:10.1029/2003JD003648.

Sassi, F., R. R. Garcia, B. A. Boville, and H. Liu (2002), On temperature inversions and the mesospheric surf zone, *J. Geophys. Res.*, *107*(D19), 4380, doi:10.1029/2001JD001525.

Sassi, F., B. Boville, D. Kinnison, and R. Garcia (2005), The effects of interactive ozone chemistry on simulations of the middle atmosphere, *Geophys. Res. Lett.*, *32*, L07811, doi:10.1029/2004GL022131.

Schmidt, H. G., et al. (2006), The HAMMONIA Chemistry Climate Model: Sensitivity of the mesopause region to the 11-year solar cycle and CO_2 doubling, *J. Clim.*, *19*, 3903–3931, doi:10.1175/JCLI3829.1.

Shettle, E. P., G. E. Thomas, J. J. Olivero, W. F. J. Evans, D. J. Debrestian, and L. Chardon (2002), Three-satellite comparison of polar mesospheric clouds: Evidence for long-term change, *J. Geophys. Res.*, *107*(D12), 4134, doi:10.1029/2001JD000668.

Swinbank, R., and D. A. Ortland (2003), Compilation of wind data for the Upper Atmosphere Research Satellite (UARS) Reference Atmosphere Project, *J. Geophys. Res.*, *108*(D19), 4615, doi:10.1029/2002JD003135.

Thomas, G. E. (2003), Are nonctilucent clouds harbingers of global change in the middle atmosphere?, *Adv. Space Res.*, *32*, 1737–1746.

Uppala, S., et al. (2005), The ERA-40 re-analysis, *Q.J.R. Meteorol. Soc.*, *131*, 2961–3012.

Xu, J., H.-L. Liu, W. Yuan, A. K. Smith, R. G. Roble, C. J. Mertens, J. M. Russell III, and M. G. Mlynczak (2007), Mesopause structure from Thermosphere, Ionosphere, Mesosphere, Energetics, and Dynamics (TIMED)/Sounding of the Atmosphere Using Broadband Emission Radiometry (SABER) observations, *J. Geophys. Res.*, *112*, D09102, doi:10.1029/2006JD007711.

C. A. Fischer, J. H. Richter, and F. Sassi, CGD/NCAR, P.O. Box 3000, Boulder, CO 80307, USA. (jrichter@ucar.edu)

R. R. Garcia and K. Matthes, Atmospheric Chemistry Division, National Center for Atmospheric Research, Boulder, CO 80307, USA.